NeuroImage 168 (2018) 222–241

Contents lists available at ScienceDirect

NeuroImage

journal homepage: www.elsevier.com/locate/neuroimage

Magnetization Transfer Contrast and Chemical Exchange Saturation Transfer MRI. Features and analysis of the field-dependent saturation spectrum☆

Peter C.M. van Zijl[a,b,*], Wilfred W. Lam[c], Jiadi Xu[a,b], Linda Knutsson[a,d], Greg J. Stanisz[c,e,f,**]

[a] The Russell H. Morgan Department of Radiology and Radiological Science, Division of MR Research, The Johns Hopkins University School of Medicine, Baltimore, MD, USA
[b] F.M. Kirby Research Center for Functional Brain Imaging, Kennedy Krieger Institute, Baltimore, MD, USA
[c] Physical Sciences, Sunnybrook Research Institute, Toronto, ON, Canada
[d] Department of Medical Radiation Physics, Lund University, Lund, Sweden
[e] Department of Medical Biophysics, University of Toronto, Toronto, ON, Canada
[f] Department of Neurosurgery and Pediatric Neurosurgery, Medical University of Lublin, Lublin, Poland

ARTICLE INFO

Keywords:
CEST
MTC
Magnetization transfer
Nuclear Overhauser enhancement
NOE

ABSTRACT

Magnetization Transfer Contrast (MTC) and Chemical Exchange Saturation Transfer (CEST) experiments measure the transfer of magnetization from molecular protons to the solvent water protons, an effect that becomes apparent as an MRI signal loss ("saturation"). This allows molecular information to be accessed with the enhanced sensitivity of MRI. In analogy to Magnetic Resonance Spectroscopy (MRS), these saturation data are presented as a function of the chemical shift of participating proton groups, e.g. OH, NH, NH_2, which is called a Z-spectrum. In tissue, these Z-spectra contain the convolution of multiple saturation transfer effects, including nuclear Overhauser enhancements (NOEs) and chemical exchange contributions from protons in semi-solid and mobile macromolecules or tissue metabolites. As a consequence, their appearance depends on the magnetic field strength (B_0) and pulse sequence parameters such as B_1 strength, pulse shape and length, and interpulse delay, which presents a major problem for quantification and reproducibility of MTC and CEST effects.

The use of higher B_0 can bring several advantages. In addition to higher detection sensitivity (signal-to-noise ratio, SNR), both MTC and CEST studies benefit from longer water T_1 allowing the saturation transferred to water to be retained longer. While MTC studies are non-specific at any field strength, CEST specificity is expected to increase at higher field because of a larger chemical shift dispersion of the resonances of interest (similar to MRS). In addition, shifting to a slower exchange regime at higher B_0 facilitates improved detection of the guanidinium protons of creatine and the inherently broad resonances of the amine protons in glutamate and the hydroxyl protons in myoinositol, glycogen, and glucosaminoglycans. Finally, due to the higher mobility of the contributing protons in CEST versus MTC, many new pulse sequences can be designed to more specifically edit for CEST signals and to remove MTC contributions.

Introduction

The average MRI signal in a voxel reflects contributions from all composing tissue compartments and provides information about the local magnetic, chemical and physical interactions that the water protons (nuclei or spins) undergo when the spin system evolves during a Magnetic Resonance (MR) experiment. Physical and chemical effects include diffusion, flow, substrate binding, and exchange of protons or water molecules between different tissue compartments or between molecules. The water protons therefore inherently report on the macroscopic and microscopic organization of tissue because they experience contact with cell organelles, cellular membranes, proteins,

☆ Contract grant sponsor: National Institutes of Health: Contract grant nos. R01EB019934, P41EB015909 and P50CA103175. Swedish Research Council Grant no. 2015-04170 and the Swedish Cancer Society 2015/251, Canadian Institutes of Health Research Grant no. PJT148660.

* Correspondence to: Johns Hopkins University School of Medicine/Kennedy Krieger Research Institute, Dept. of Radiology/F.M. Kirby Research Center, 707 N. Broadway, Baltimore, MD 21205, USA.
** Correspondence to: Sunnybrook Health Science Centre, 2075 Bayview Ave., Room S6 72, Toronto, ON, Canada M4N 3M5.
E-mail addresses: pvanzijl@mri.jhu.edu (P.C.M. van Zijl), stanisz@sri.utoronto.ca (G.J. Stanisz).

http://dx.doi.org/10.1016/j.neuroimage.2017.04.045
Accepted 19 April 2017
Available online 21 April 2017

DNA, cellular metabolites, blood components, etc. For instance, relaxation properties are affected by water motion, which may vary from almost free, e.g. in the cytoplasm, to severely restricted, e.g. when temporarily trapped in a semi-solid environment such as a membrane. In addition, protons are magnetic dipoles (spins) that will interact with other spins in their environment either through the electrons in the chemical bonds (called scalar coupling) of molecules or through space via dipolar coupling. During these physical, chemical and magnetic interactions, magnetization can be transferred between different locations within the molecule or between molecules. When performing imaging experiments, all of these effects contribute to the signal intensities and tissue parameters measured, e.g. relaxation times and diffusion constants. While this complicates the interpretation of MR images, it also provides the foundation for the versatility of this technology to study multiple aspects of tissue physiology simply by varying some pulse sequence parameters.

In this review we discuss the transfer of magnetization between spin systems that undergo chemical exchange and experience dipolar coupling effects with nearby nuclear systems and how such interactions are assessed in conventional Magnetization Transfer Contrast (MTC) and in Chemical Exchange Saturation Transfer (CEST) MRI experiments. The historical nomenclature for these two technologies is unfortunately a bit confusing, because all of these processes fall under the general Nuclear Magnetic Resonance (NMR) category of magnetization transfer (MT) and, due to the similar principles and pulse sequences employed, these effects are generally mixed. The magnetization of the molecular proton pool can be affected either by radio-frequency (RF) saturation, i.e. equilibration of the spin populations in the proton energy states resulting in removal of detectable magnetization, or RF excitation, i.e. interchanging of the spin populations of the energy states, which can lead to different types of transverse and longitudinal magnetization and multiple- or zero-quantum spin coherences. In solid-like molecules, excitation always also leads to removal of detectable signal, because of rapid dephasing of any transverse magnetization generated due to the microsecond proton T_2. As a consequence, MTC experiments have a featureless broad Z-spectrum and are limited to saturation transfer. However, in mobile molecules transverse magnetization and spin coherences stay around, giving rise to the possibility of spin system manipulations (chemical shift evolution, use of spin coherence selection) similar to high resolution NMR. As such CEST has an unlimited potential for editing of spectral components and visualizing spin systems before their ultimate detection as saturation on the water signal.

In this review, we will first provide a brief explanation of the phenomena underlying magnetization transfer, namely chemical exchange, the nuclear Overhauser enhancement (NOE) and the effects of dipolar transfer. We then proceed to an explanation of CEST basics, followed by an introduction of the Z-spectrum, typically used to measure CEST and MTC effects. We will then discuss the details of the in vivo Z-spectrum, including the contribution of relayed NOEs in mobile macromolecules. These three phenomena and the occurrence of direct water saturation (DS; also known as the direct effect, DE, in MTC literature) all mix when irradiating within the basic frequency range of the proton spectrum of solute molecules (metabolites, proteins, peptides, etc.). The contributions of these components change as a function of B_0, B_1 and the RF pulse shape and sequence timing, which has to be kept in mind when analyzing CEST images. Especially important is the coalescence of lineshapes with the water proton resonance for compounds containing fast exchanging proton groups such as the amines and hydroxyls in compounds like glutamate and myoinositol. Here, we will highlight how the move to stronger B_0 fields can enhance the information measured in CEST images and discuss the current status of the development of approaches to separate out spectral components.

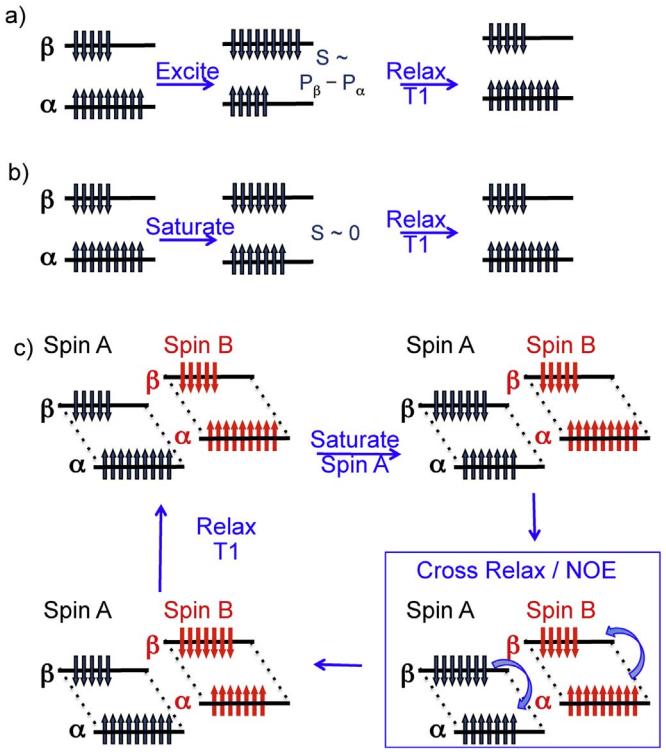

Fig. 1. Schematic overview of the effect of (a) excitation, (b) saturation and (c) cross-relaxation (NOE) on the proton spin pool populating the proton energy levels. The difference in spin population (P) between energy levels is ~1–10 per million, leading to a resultant polarization (a) that can be detected (signal S) after excitation. Saturation minimizes the resultant polarization (b). When two protons (A and B) are coupled, their populations can cross-relax and saturation of one spin pool can the transferred to the other (c). The effect shown here is for slow-moving molecules, leading to reduction in polarization in the neighboring spin or a negative NOE.

Magnetization transfer processes in semisolid and mobile macromolecules

In order to understand CEST and MTC experiments and their close relationship, it is essential to have a basic understanding of transfer of polarization between nuclei. When protons are placed in a magnetic field, they attain two energy levels (Fig. 1a, E_α and E_β). The lower level (spin up, α) is slightly more populated (P_α) than the higher level (spin down, β, with P_β). Polarization is the difference in population between the two energy levels that a pool of spins attains in a magnetic field. The magnetization detected in MRI is proportional to that, and, because it is determined by the Boltzmann distribution at physiological temperature, it is very small (~1–10 per million, depending on B_0), which is the origin of the low sensitivity of MRI. To detect a signal S, the spin system is excited (Fig. 1a) after which it relaxes back to equilibrium with T_1. When continuously irradiating a spin pool using RF, such as in MTC or most CEST experiments, the populations equilibrate (Fig. 1b). Thus while the total number of spins remains the same, there is no residual longitudinal magnetization and if we subsequently excite the spin system, the signal will be negligible. Such saturation can be transferred between molecules if the protons exchange physically between them, allowing us to benefit from the CEST method. However, there is an additional mechanism that can cause such polarization transfer even if protons don't exchange. This occurs when a through-space dipolar coupling exists between neighboring spins, which allows the spins to relax not only with T_1 but also with a much faster cross-relaxation rate. The strength of the dipolar coupling depends on the distance r between the nuclei ($\sim 1/r^3$), their gyromag-

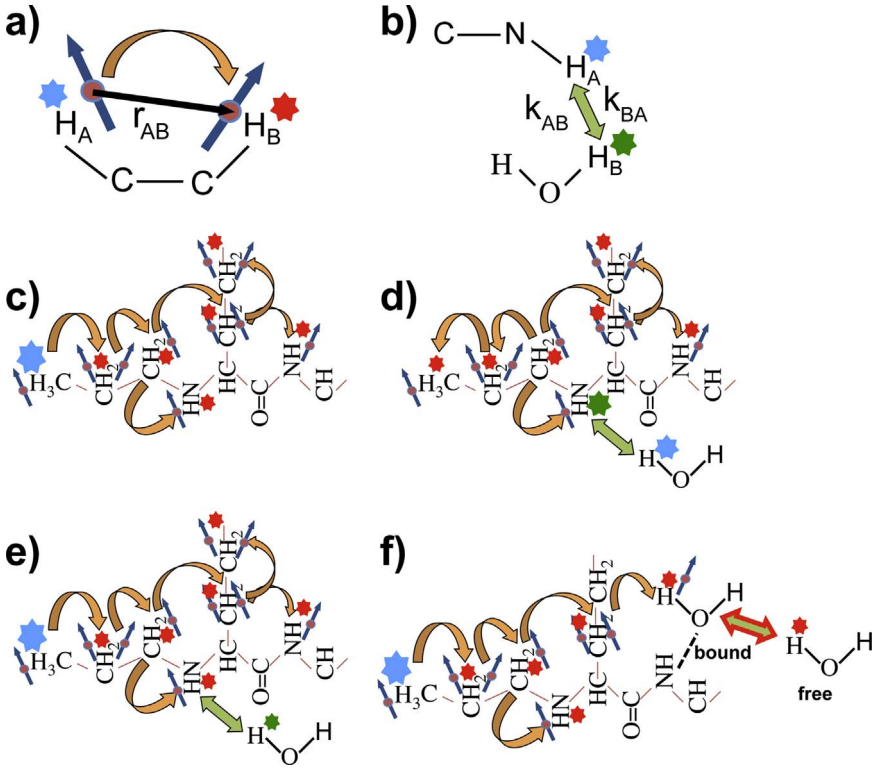

Fig. 2. Nomenclature and terminology for polarization (magnetization) transfer. The blue star indicates where the protons are labeled using either excitation or saturation; the red star indicates after dipolar transfer; the green star after chemical exchange. a) Dipolar transfer between protons that have dipole-dipole coupling $D \sim \gamma_A \gamma_B / r_{AB}^3$ and can undergo cross-relaxation (orange arrow), which is proportional to D^2 and the motional correlation time, causing NOE in a neighboring proton. b) Chemical exchange with rate equilibrium dependent on pool sizes: $M_A k_{AB} = M_B k_{BA}$; c) relayed dipolar transfer (relayed NOE or spin diffusion); d) exchange-relayed NOE; e) NOE-relayed (rNOE) exchange, such as occurs in the upfield (lower frequency region of CEST spectra); f) intramolecular NOE-relayed transfer followed by intermolecular NOE to bound water, followed by either molecular (water) exchange or proton exchange to free water. (For interpretation of the references to color in this figure legend, the reader is referred to the web version of this article.)

netic ratios and their relative orientation. Contrary to scalar coupling which can be seen in the proton spectrum, its visibility in an MR experiment depends on motion and because of fast molecular tumbling in liquids it is averaged out and not detectable. However, cross relaxation between dipolar coupled nuclei is always present and increases with reduction in rotational motion, e.g. going from small molecules to mobile macromolecules, and becomes extremely efficient in semi-solid tissue structures such as cellular membranes. Under such conditions, when saturating a spin pool A, the polarization of a spin pool B coupled to it can flip due to cross relaxation, while pool A returns back to its original polarization (Fig. 1c). Thus, saturation or excitation can be transferred. NOE is a transfer of polarization from one pool of spins to another via cross-relaxation due to the existence of a dipolar coupling between the two pools (Solomon, 1955). This effect spreads the polarization throughout the molecule (a process called spin diffusion) and underlies the MTC phenomenon used in MRI as well as the NOE effects of macromolecules contributing to the CEST effect. Notice that this process has to be faster than T_1 to be measurable.

The terminology that should be used for the above transfer processes is explained in Fig. 2. After a proton is magnetically labeled (blue star), i.e. it no longer has equilibrium polarization (Fig. 1a,b), its polarization can be transferred to neighboring protons either using dipolar coupling and resulting cross-relaxation (NOE, Fig. 2a) or using chemical exchange (Fig. 2b). When molecular motion is sufficiently slow, these NOEs can be relayed through the backbone of macromolecules with an efficiency that increases with reduced motion (Fig. 2c). If water is saturated, for instance in proton spectroscopy or inverted such as in the water exchange (WEX) experiment (Mori et al., 1996a), which is the inverse of the CEST experiment, saturation or magnetization can be transferred through exchange to solutes, after which it can be relayed further throughout the macromolecule with NOEs (Mori et al., 1996b) (Fig. 2d), which is called an exchange-relayed NOE. Alternatively, when saturating or exciting the backbone of a mobile macromolecule, this magnetization can be relayed to an exchangeable proton, which can then go to the water. This so-called NOE-relayed (rNOE) exchange (Fig. 2e) is a major source of the upfield narrower NOE signals seen in the Z-spectra in CEST experiments, which will be discussed in more detail in the next sections. Finally, when saturating any proton pool of a semi-solid tissue component, the saturation is relayed rapidly with NOEs and can be transferred efficiently through space to protons of bound water molecules (Fig. 2f). Notice that this intermolecular NOE transfer to bound water, which is assumed to be the main mechanism in MTC experiments (Edzes and Samulski, 1977; Wolff and Balaban, 1989), is very efficient in the solid-like environment, but negligible in mobile proteins (Hwang et al., 1998; Otting et al., 1991), which is sometimes confused in the literature. The saturated water can subsequently exchange with free water molecules either through water exchange or proton exchange, which is why we colored the arrow in Fig. 2f both green and red. Of course saturation in the semi-solid can also be transferred rapidly to water through exchangeable protons (Liepinsh and Otting, 1996), such as the cerebroside hydroxyl protons in myelin. So both mechanisms contribute to semi-solid based transfer, but not to transfer from mobile proteins.

In tissue these polarization transfer or magnetization transfer effects all occur simultaneously when the particular spins of different tissue components resonate at the same frequency and contribute to the Z-spectrum in a manner dependent on molecular motion, exchange rate, the applied B_0 and B_1 fields, and molecular interaction.

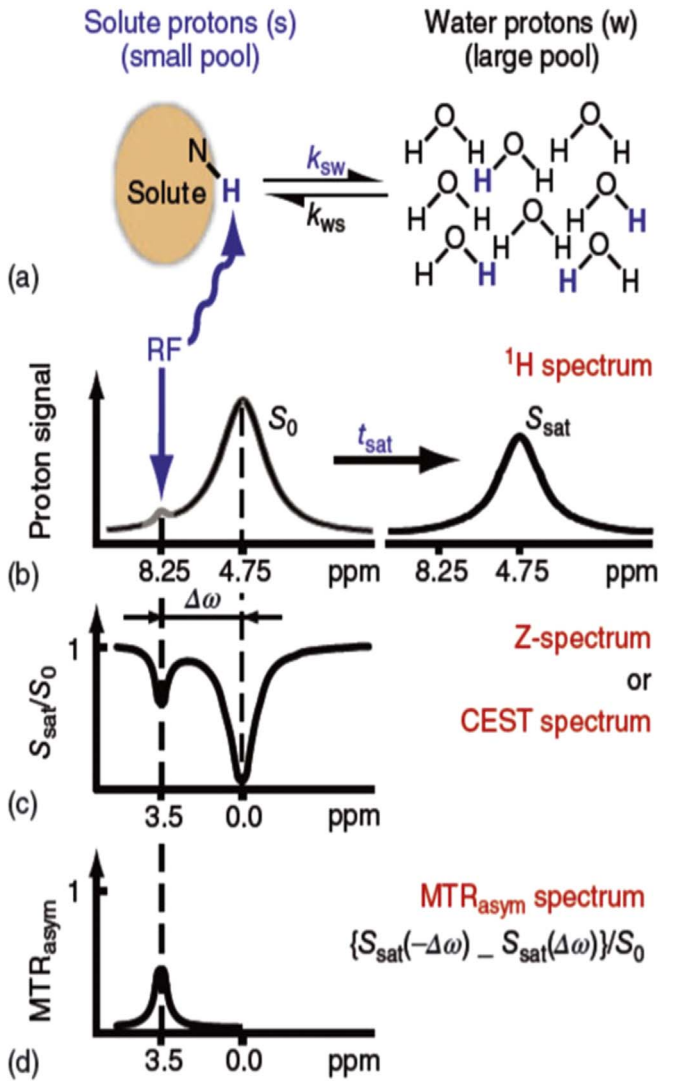

Fig. 3. Chemical Exchange Saturation Transfer (CEST). (a,b) Solute protons (blue) are saturated at their specific resonance frequency in the proton spectrum (here 8.25 ppm for amide protons). This saturation is transferred to water (4.75 ppm) with exchange rate k_{sw} and non-saturated protons (black) return. After a saturation period (t_{sat}), this effect becomes visible on the water signal (b, right). (c) The Z-spectrum, showing normalized water saturation (S_{sat}/S_0) as a function of irradiation frequency. When irradiating the water protons at 4.75 ppm, the signal disappears due to direct (water) saturation. This frequency is assigned to 0 ppm in Z-spectra. At short saturation times, only this direct saturation is apparent. At longer t_{sat} the CEST effect becomes visible at the frequency of the low-concentration exchangeable solute protons, now visible at 8.25–4.75=3.5 ppm in the Z-spectrum. (d) Result of Magnetization Transfer Ratio asymmetry (MTR_{asym}) analysis of the Z-spectrum with respect to the water frequency to remove the effect of direct saturation. Reproduced, with permission from van Zijl & Yadav, Magn. Reson. Med. 65, 927 (2011). (For interpretation of the references to color in this figure legend, the reader is referred to the web version of this article.)

Basics of CEST MRI

The principle of intermolecular saturation transfer using exchangeable protons, such as those in hydroxyl (OH), amide or imino (NH), amine (NH_2) or thiol (SH) groups, was first demonstrated in the sixties (Forsen and Hoffman, 1963). CEST MRI was named (Ward et al., 2000) to describe the transfer of such saturated protons from metabolites and contrast agents to water protons via the exchange of protons between molecules. The crucial features introduced were that MRI could now be used for detection and that a large sensitivity enhancement could be obtained. CEST MRI is analogous to MRS (van Zijl and Sehgal, 2016) in that multiple proton groups at different resonance frequencies can be studied. While the most important feature of MRS is its molecular specificity, it is generally hampered by very low sensitivity because of the millimolar concentration of the directly detected proton pools. CEST provides increased sensitivity at the cost of reduced specificity, because the exchangeable proton resonances are generally wider than those from the aliphatic protons and the saturation lines have linewidth proportional to B_1. However, CEST does provide molecular specificity with MRI sensitivity, which explains the great interest in this rapidly expanding field.

A pictorial description of the CEST mechanism is shown in Fig. 3 (van Zijl and Yadav, 2011). In short, the exchangeable proton pool of a solute is saturated using a RF pulse at the specific resonance frequency of these protons. When exchange occurs with water protons, the water signal will be slightly reduced, i.e. on the order of the concentration of the solute protons (millimolar), but this would not be detectable with respect to the 110 M water proton signal in MRI due to limited dynamic range. The main strength of CEST comes from the fact that the unsaturated protons from the water that replace the removed saturated solute protons will get saturated by the RF irradiation, and that this process repeats itself to build up an increasing signal loss on water. When the exchange rate from the solute "s" to water (k_{sw}) is on the correct order of magnitude compared to the efficiency of saturation (α_s), signal enhancements by a factor of 100–1000 or even more can be achieved (Aime et al., 2009; Goffeney et al., 2001; Sherry and Woods, 2008; Ward et al., 2000; Woessner et al., 2005; Zhou et al., 2004). However there are some conditions to be met for this to be done successfully. The solute proton pool must have a sufficiently fast exchange rate (k_{sw}) to the water proton pool "w" and be sufficiently saturated before exchange occurs. Other favorable conditions are (i) for the saturated water protons to have a long T_1 to allow the saturation to remain and (ii) for the exchange regime to be in the slow to intermediate range, i.e., $\Delta\omega_{sw} \geq k_{sw}$, in which $\Delta\omega$ is the frequency difference with water in radians/s. The latter causes the chemical shift of the proton in the solute pool to be sufficiently separated from that of water, improving selectivity. When assuming a slow exchange regime and a two-pool model with no back exchange of the saturated protons or perturbation from the RF irradiation to the water protons, a simplified analytical expression of the proton transfer ratio (PTR) can be obtained for the CEST effect (Goffeney et al., 2001; Zaiss and Bachert, 2013a; Zhou et al., 2004):

$$PTR = x_s \cdot \alpha_s \cdot k_{sw} \cdot T_{1w}(1 - e^{-t_{sat}/T_{1w}}) \quad (1)$$

in which

$$x_s = \frac{[exchangable\ protons]}{[water\ protons]} = \frac{k_{ws}}{k_{sw}} \quad (2)$$

Here, square brackets indicate concentration and x_s is the fraction of solute protons, T_{1w} the T_1 of water, and t_{sat} the saturation duration. Thus the CEST effect increases with the relative concentration of solute protons, the saturation efficiency of the RF pulse, and the exchange rate. However, the two T_{1w} terms partially compensate each other.

Basics of MTC MRI

Conventional Magnetization Transfer Contrast imaging of semi-solid systems, which we will define as MTC here because MT is too general of a concept as explained above, refers to the phenomenon that application of a RF saturation pulse at a frequency well outside the proton NMR spectral range (~0–10 ppm with water around 4.75 ppm in MRS) causes a reduction in the water signal. This was first discovered in vivo in the eighties (Wolff and Balaban, 1989) and studied and reviewed in detail in the following decade (Balaban and Ceckler, 1992; Henkelman et al., 1993, 2001; Pike, 1996; Stanisz et al., 1999, 2005; Wolff and Balaban, 1989). The reason for this effect is that this far off-resonance RF pulse (i.e. from water), while not affecting the proton spectrum of mobile tissue compounds including water, is

partially saturating the proton pools of semi-solid tissue components (e.g. membranes or myelin sheets) that have very short T_2 and exhibit large dipolar couplings. The width of these resonances is so large that they can still be irradiated at frequencies that extend well beyond the proton spectral range in liquids. This saturation can be transferred rapidly through the solid-like system and eventually to the water protons (Edzes and Samulski, 1977; Wolff and Balaban, 1989).

Definition and features of the Z-spectrum: direct water saturation effect (DE), MTC, CEST, and relayed NOEs of mobile proteins; effects of $B_1$and B_0

To measure saturation effects, a Z-spectrum (Bryant, 1996; Guivel-Scharen et al., 1998) is acquired in which the water signal intensity during saturation (S_{sat}) is normalized to the signal intensity without any saturation (S_0) and displayed as a function of the saturation frequency (Fig. 3c). A significant reduction in water signal occurs after irradiation at a frequency offset that corresponds to the resonance of the solute protons. A very important point to notice is that Z-spectra are referenced to the water proton frequency assigned to 0 ppm, while the water frequency in the ^{1}H MRS spectrum (Fig. 3b) is around 4.75 ppm due to the use of tetramethylsilane (TMS) and trimethylsilylpropanoic acid (TSP) as references for 0 ppm *in vitro* and *in vivo*, respectively. Also important is that the correct convention for the spectrum is to have positive frequencies on the left, since it is based on correspondence to the proton spectrum.

Since both MTC and CEST MRI use molecular proton saturation and water detection, these phenomena mix in the resulting image when irradiating within the basic frequency range of the proton spectrum of solute molecules (metabolites, proteins, peptides, lipids, etc.). This mixing makes the interpretation of the data from saturation experiments confusing since it is often challenging to separate different contributions (DE, MTC, and CEST) in measured Z-spectra. To make things worse, the degree to which different kinds of molecular protons contribute at each frequency depends on the magnetic field strength B_0, the B_1 field used, the number of saturation pulses and their shape, and the pulse sequence timing. It also strongly depends on intrinsic relaxation properties of proton pools and exchange rates. In order to further comprehend the influence of these different contributions on the Z-spectrum we discuss them in order of their relative dominance.

Direct effect

When there are no macromolecules or solutes interfering (i.e., in the absence of MTC and CEST), the effect of direct RF saturation of water protons is readily described by the Bloch equations (Henkelman et al., 1993). The normalized signal $S_{sat}(\Delta\omega)/S_0$ is minimal when the RF saturation occurs at the water resonance frequency and unity far off resonance. The offset $\Delta\omega$ is given in absolute or relative units (Hz and ppm, respectively) from the water proton pool's resonance frequency, defined to be at 0 Hz and 0 ppm, respectively. The former is useful for specifying RF saturation frequencies on scanner hardware (and used usually in MTC literature) while the latter facilitates comparison of spectra independent of field strength (standard in NMR, MRS and for describing CEST phenomena). The use of these two different conventions may lead to confusing results between laboratories as we demonstrate below (Fig. 4).

Fig. 4a, using the MTC frequency convention, shows the simulated DE in gray matter (see Table 1 for exchange parameters) for two different saturation RF powers (B_1=1 and 4 μT) and three external magnetic fields (1.5, 3, and 7 T). The direct saturation spectrum around 0 Hz (0 ppm) is a Lorentzian (Mulkern and Williams, 1993; Wolff and Balaban, 1989) with a linewidth $\Delta_{½\ max}$ at half maximum saturation increasing linearly with the RF saturation frequency $\omega_1=\gamma B_1$ and given by:

$$\Delta_{\frac{1}{2}\max} = \frac{\omega_1}{\pi}\sqrt{\frac{T_{1w}}{T_{2w}}} \quad (3)$$

Where T_{1w} and T_{2w} are the longitudinal and transverse relaxation times of the water pool, respectively. The DE spectrum in Hz widens with increased B_0 field, due to an increase in the T_{1w}/T_{2w} ratio, since T_{1w} increases with magnetic field (Bottomley et al., 1984), while T_{2w} slightly decreases or remains constant (Bottomley et al., 1984; Stanisz et al., 2005). However, the saturation line narrows when using the NMR ppm scale (Fig. 4c), which indicates that separation of spectral components is expected to improve at higher field, as is well known in the NMR and MRS fields.

The CEST effect can sometimes be diminished by the direct effect (DE) of water saturation, namely when the solute protons resonate close to the water frequency or when using a strong B_1. Assuming that DE is symmetric around the water resonance, the water signal reduction due to CEST effects can be visualized by the subtraction of one image with a selective saturation RF pulse on the solute protons and another one with saturation on the opposite side of the water resonance. This reconstruction approach (Fig. 3d) is called MT ratio asymmetry (MTR_{asym}) analysis. Using the definition $MTR=1-S_{sat}/S_0$, this process is characterized by:

$$MTR_{asym}(\Delta\omega) = MTR(\Delta\omega) - MTR(-\Delta\omega) = \frac{S_{sat}(-\Delta\omega)}{S_0} - \frac{S_{sat}(\Delta\omega)}{S_0} \quad (4)$$

Alternatively, $S_{sat}(\Delta\omega)$ has been used for normalization instead of S_0. However, when using asymmetry analysis, it has to be realized that all saturation transfer effects that are not symmetric with respect to the water resonance will still contribute, which will be discussed in detail below.

Contribution of MTC

To properly describe effects *in vivo* in tissue, the exchange process between the very broad semisolid macromolecular MTC pool (T_2 on the order of microseconds) and the free water pool has to be added in. Conventionally in the MTC field it has been assumed that the solid-like macromolecular pool line shape is symmetric around water at 0 Hz (or 0 ppm), probably due to the dominance of the direct saturation of this resonance, and can be described as super-Lorentzian (Morrison et al., 1995). Addition of such a symmetric semisolid pool, which is in magnetic contact with water, causes an apparent overall signal attenuation (Fig. 4b) that quickly becomes dominant at high saturation powers. Note that MTC parameters such as semisolid fraction and exchange rate are field independent, while the T_2 relaxation of the macromolecular pool is so short that no effect is apparent with the B_0 field. Therefore, when using the frequency scale and assuming a single MTC component symmetrical with respect to the water frequency, the difference between MTC spectra across different magnetic fields B_0 can be assumed to be driven mainly by changes in T_{1w}/T_{2w} ratio, i.e., the spectrum of the direct effect. In recent years there has been an increasing number of reports indicating that the MTC effect is not symmetric (Hua et al., 2007; Pekar et al., 1996; Swanson and Pang, 2003; Swanson et al., 2016). The issue whether MTC is symmetric or not has been a matter of sometimes heated debate. We will discuss this problem at the end of this section and after the experimental data section, since, in our view, one cannot discuss MTC asymmetry without the presence of CEST effects, which dominate at low B_1-values, and the truth can only be determined by experimental data.

CEST and rNOEs of mobile proteins and peptides

Additional features in the Z-spectrum occur because of magnetization transfer to water from proton pools in dissolved proteins and peptides, amino acids, sugars, and other metabolites, which are the typical CEST pools. The amount of attenuation observed from a given

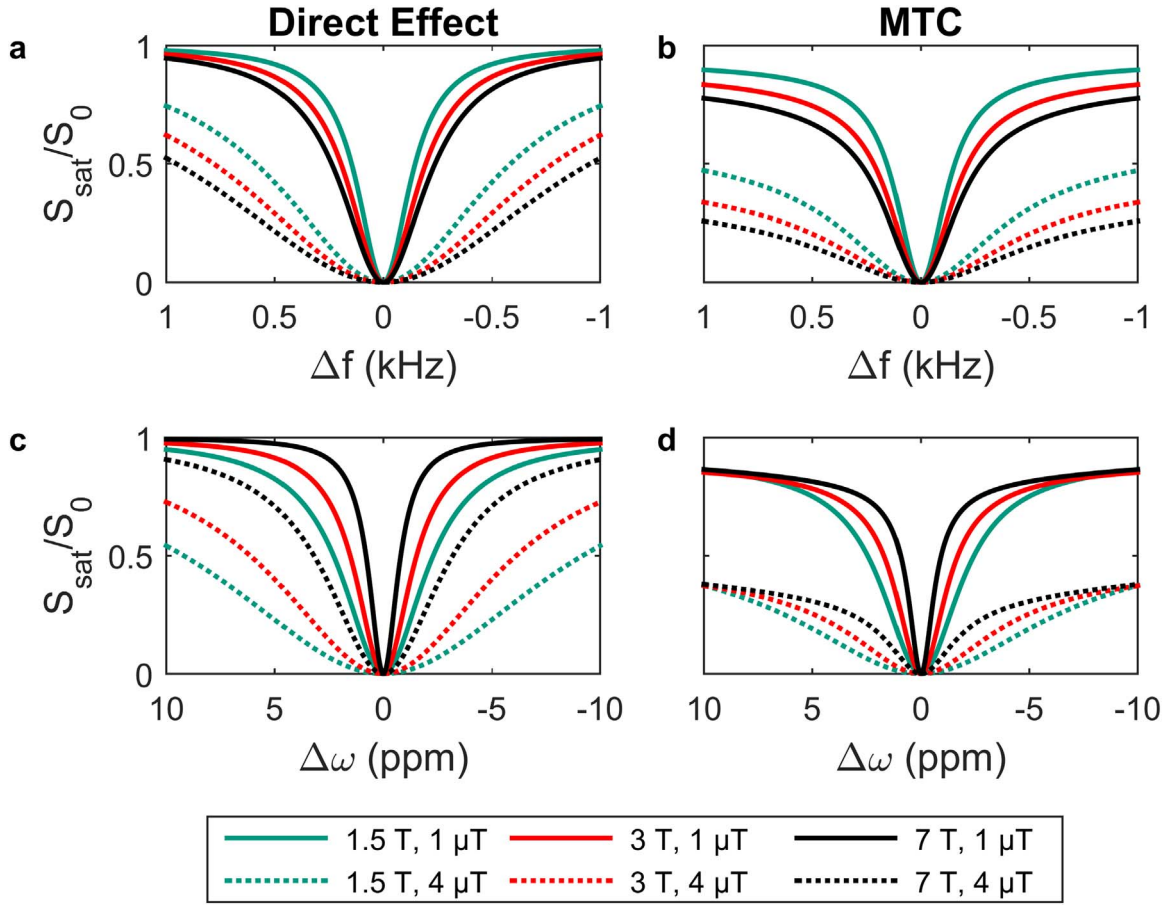

Fig. 4. Simulated direct effect (a,c) and symmetric MTC (b,d) using frequency scale (kHz) convention (a,b) from MTC and the NMR (CEST) convention in ppm (c,d). These spectra assume a hypothetical case of gray matter at different field strengths B_0 and for different saturation pulse amplitudes B_1. Note that, due to the use of symmetric MTC, the different spectral appearances as a function of B_0 in a and c are due mainly to T_{1w} and T_{2w}. The same is true for c and d, but due to the increase with field in frequency/ppm being larger than the increase in the square root of T1w/T2w, the saturation lines narrow with field. Parameters used: T_{1w}=0.8, 1.2, 1.6 s, T_{2w}=72, 69, 62 ms (at 1.5, 3, 7 T, respectively); MTC: fraction 5%, rate 40 Hz, T_1=1 s, T_2=9 μs, steady state continuous saturation.

Table 1
Exchange parameters for simulations.

	Offset vs water (ppm)	Exchange rate k_{sw} (Hz)	Proton Concentration (mM)	T_2 (ms)
MTC (Gray matter)	0	40	5500	0.009
CEST, amide	3.5	30	72	100
CEST, amine (glutamate)	3	5500	20	200
CEST, guanidinium (creatine)	2	1100	20	170
CEST, hydroxyl (myo-inositol)	0.9	2000	45	55
rNOE 1	-1.75	16	100	5
rNOE 2	-2.25	16	100	5
rNOE 3	-2.75	16	100	5
rNOE 4	-3.25	16	100	5
rNOE 5	-3.75	16	100	5

Note that the exchange rate is for exchange from the solute "s" to water "w" pool.

pool is dependent on its exchange rate with water (which, in turn, is dependent on temperature, pH, proton shielding, and mobility). Exchangeable proton effects are typically seen at frequencies higher than the water proton resonance (i.e. downfield from water). A commonly investigated CEST proton pool is that of amides in the backbone of dissolved proteins centered at around 3.5 ppm (Goffeney et al., 2001; Zhou et al., 2003a, 2003b). Another pool includes primary amine groups and guanidinium proton groups, especially but not exclusively in amino acids, with chemical shifts ranging from about 2 to 3 ppm. Examples include glutamate (Cai et al., 2012) in the brain and creatine (Haris et al., 2012) in brain and muscle. Another major pool is that of hydroxyl protons in sugars from around 0 to 3.5 ppm, especially myo-inositol in the brain (Haris et al., 2011) and glycogen in liver and muscle (van Zijl et al., 2007). In the knee, the hydroxyl group of glycosaminoglycans has been studied (Ling et al., 2008). Shift differences may be much larger if the protons are hydrogen bonded (Lauzon et al., 2011; Yang et al., 2013), but these have not yet been found *in vivo*. A list of some CEST agents and their relevant parameters can be found in (Ward et al., 2000; Zhou and van Zijl, 2006), but it has to be kept in mind that this is a subset, as any compound with exchangeable protons can, in principle, be a CEST agent and contribute to the Z-spectrum.

In addition to signals downfield, typically features are visible in the negative frequency offset (upfield) region of the Z-spectrum (Ling et al., 2008; van Zijl and Yadav, 2011). A local minimum commonly seen in cancer cells (Desmond et al., 2014; Jones et al., 2013) and the brain (Heo et al., 2016a, 2016b, 2016c; Jin et al., 2013; Jones et al., 2013) occurs at approximately –(2.0–3.5) ppm, corresponding to the frequency offset of tertiary, secondary and primary aliphatic groups (i.e., having chemical formulas of R_3CH, R_2CH_2, and R_2CH_3 respectively). Another prominent rNOE has recently been demonstrated at -1.6 ppm, assigned to choline phospholipids (Zhang et al., 2016a, 2016b). Data from water-exchange (WEX) filter spectroscopy experiments (van Zijl

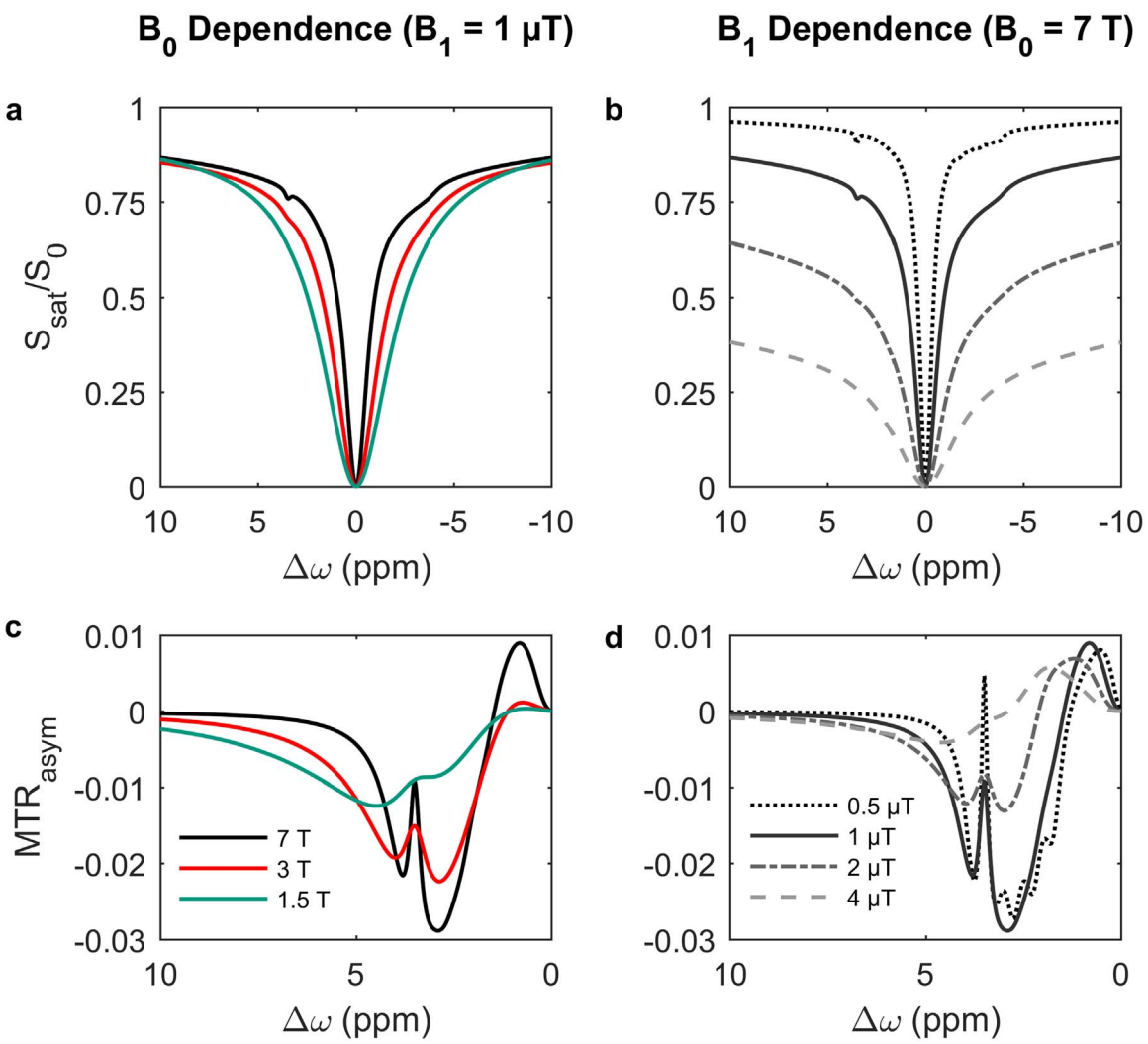

Fig. 5. Simulated Z-spectra of gray matter including CEST contributions as a function of B_0 (a,c) and B_1 (b,d). The B_0 fields for (a,c) are indicated in (c) and the B_1 fields for (b,d) in (d). These spectra include the direct effect and symmetric MTC contributions described in Fig. 4. As per NMR (and MRS, CEST) convention the frequency offsets are in ppm. CEST components: amide (3.5 ppm, 72 mM, k_{sw}=30 Hz, T_2=100 ms), glutamate (3 ppm, 20 mM protons, k_{sw}=5500 Hz, T_2=200 ms), creatine (2 ppm, 20 mM protons, k_{sw}=1100 Hz, T_2=170 ms), myo-inositol (0.9 ppm, 45 mM protons, k_{sw}=2000 Hz, T_2=55 ms), and five NOE components -1.75, -2.25, -2.75, -3.25, and -3.75 ppm; each 100 mM protons, k_{sw}=16 Hz, T_2=5 ms).

et al., 2003) show that this magnetization loss in the Z-spectrum originates from these groups via intramolecular rNOEs to backbone amide protons, which subsequently exchange with water protons, but not from direct dipolar effects between water and the macromolecules (Hwang et al., 1998; Otting et al., 1991). Several different resonances of mobile macromolecules are present in this frequency range, but they often appear as a continuous broad line in Z-spectra, most likely due to the interference from the NOEs from the MTC effect. Only at very low B_1 can these spectral fine structures be distinguished (Jones et al., 2013). These mobile macromolecular features are also visible in short-TE proton spectra (Behar et al., 1994; Kauppinen et al., 1993).

Fig. 5 shows simulated, illustrative Z-spectra for gray matter including CEST contributions consisting of amide (3.5 ppm), amine (glutamate, 3 ppm), guanidinium (creatine, 2 ppm), and hydroxyl (myo-inositol, 0.9 ppm) protons and five rNOE components (see Table 1 for shifts and exchange parameters). The presence of exchanging CEST pools and rNOEs only slightly alters the shape of the observed Z-spectrum and they become manifest only at higher B_0 values (Fig. 5a–b) and low B_1 values. At lower B_0, the contributions of these CEST and rNOE pools to the Z-spectrum are difficult to see, but they can be appreciated by the presence of the Z-spectrum asymmetry when performing MTR_{asym} analysis (Fig. 5c and d). The CEST effects are more pronounced at lower saturation pulse amplitudes as seen in Fig. 5b but the asymmetry persists (even though strongly reduced) at high powers due to removal in large part of the symmetric DE and MTC contributions.

Asymmetry in the Z-spectrum

Based on theoretical expectations and illustrated by the simple simulations in Fig. 5, it is clear that, at low B_1 (< 1 μT), the slow-exchanging CEST (e.g., amide) and rNOE contributions cause a strong asymmetry in the proton spectral range, which quickly reduces to zero just above 5 ppm. Fig. 5 also shows that one cannot neglect the effects of CEST exchange at high B_1, but that the contributions differ because the saturation of slow-exchanging protons is maximal, while that of the fast exchanging protons keeps increasing with power. Thus, even at 4 μT the simulated Z-spectrum is asymmetric, although the effects become less apparent due to the large DE and MTC contributions that cause most of the water saturation. In our simulations, we assumed symmetric MTC. After the experimental section we will discuss whether this is a realistic approach and whether, in addition to the asymmetric

CEST/rNOE effects, asymmetric MTC should be included for data interpretation at both lower and higher B_1 values.

Measuring Z-spectra

Before discussing features of Z-spectra from the literature, it is important to point out that such data are affected by the hardware used and that it is necessary to correct for influence of B_0 and B_1 inhomogeneity and system instability. For example, shimming may not be able to create a uniform B_0 field within the subject, leading to shifts in the frequency offset axis unique to each voxel. Similarly, the transmit field may not have a uniform spatial profile due to coil loading or have a systematic bias due to incorrect transmit gain calibration. These system imperfections affect the Z-spectra, because experiments use prescribed $\Delta\omega$ and ω_1 values that may differ from the actual ones at different spatial locations. Voxelwise B_0 correction can in principle be performed at low B_1 by shifting the Z-spectrum of each voxel to 0 ppm using the DE (Stancanello et al., 2008), but at higher B_1, this simple approach is prone to error *in vivo* as interference of hydroxyl groups may broaden the water lineshape and change the minimum. Alternatively, and more accurately, a separate B_0 assessment can be acquired, for instance using a low saturation power scan with frequency offsets centered closely about the water resonance in a technique known as water saturation shift referencing (WASSR) (Kim et al., 2009), a B_0 map with every frequency offset (Keupp and Eggers, 2010), or a two-echo B_0 map (Wei et al., 2010). Recently, a technique called WASABI was published that simultaneously allows for mapping of B_0 and B_1 (Schuenke et al., 2016).

For long scans, such as Z-spectrum acquisition with dense frequency offset sampling, there may be drift over time of the reference signal intensity S_0 leading to inaccurate normalization of the acquired signal. This can be corrected by acquiring reference scans at regular intervals during an experiment, interpolating the reference scans if necessary, and normalizing the signal acquired by this time-varying reference value (Desmond and Stanisz, 2012; Jones et al., 2013). Further, when fitting the entire Z-spectrum, Rician noise disproportionately increases the signal in low-signal frequency offsets (i.e., near the water resonance) compared to other higher-signal offsets. A signal-level-dependent subtraction based on a measurement of the background noise standard deviation can be used for correction (Henkelman, 1985).

The above system-based criteria affect quantification of CEST effects when ratiometric or signal difference approaches with respect to the water frequency (such as MTR_{asym}, Eq. (4)) are used. In the following discussion of experimental data, we have selected examples for which the appropriate corrections were performed.

Experimental Z-spectra and what they tell us

As a first example of *in situ* Z-spectra, Fig. 6 shows data acquired for the rat brain (mixture of gray and white matter) at 4.7 T under three different physiological conditions, namely normocapnia and hypercapnia *in vivo,* and postmortem (Zhou et al., 2003b). Several features become clear immediately for these data with a large MTC contribution. First, similar to the simulations, there is hardly any spectral fine structure visible, except for a small dip at the 3.5 ppm offset, attributed to the combined amide proton transfer (APT) effect. Secondly, there is a clear Z-spectral asymmetry within the proton spectral range for mobile components (0–5 ppm, Fig. 6a,b), which is not visible when looking in areas of mainly CSF (Fig. 6g), where the DE is expected to dominate. These two effects are confirmed when performing asymmetry analysis (Fig. 6c and h). Interestingly, however, the asymmetry is maintained in brain tissue when measuring well outside the spectral range for mobile molecules (Fig. 6d). More insight can be attained when looking at the different physiological conditions. While the Z-spectra for hypercapnia and normocapnia are shifted in intensity, the shape remains the same within error as revealed by the MTR_{asym} spectra in Fig. 6c and d. On the contrary, when comparing *in vivo* and postmortem, the MTR_{asym} data differ over the 2–5 ppm range, while this difference is clearly negligible outside the range for mobile molecules (Fig. 6d). The main difference immediately postmortem versus *in vivo* is acidification of the tissue, evidenced by the reported drop in pH from 7–7.1 to about 6.7, as measured with ^{31}P spectroscopy. Thus, the pH change shows a reduction in saturation transfer in the mobile molecule (CEST) spectral range, but not for the larger offsets (MTC based). This is in line with older reports showing no significant saturation transfer changes with pH for MTC. These data show a clear asymmetric contribution for MTC in the brain, and this will have to be taken into account in future simulations. Finally, Fig. 6e and f show the changes in PTR between normocapnia and hypercapnia and normocapnia and cardiac arrest. Again the postmortem data show a clear effect only in the CEST spectral range, i.e., associated with mobile molecules. The maximum effect postmortem is at an offset of 3.5 ppm, the resonance of the amide protons, leading to extensive investigations in the use of amide proton transfer (APT) for clinical application.

In Fig. 7, recent data from Lam and Stanisz (unpublished results) at 7 T for gray matter in the mouse brain are shown. Similar to the simulations, spectral features at 3.5 and 2 ppm become visible, presumably due to the amide and guanidinium (creatine) protons, respectively. At this low power of less than 1 μT, the asymmetry is determined by the CEST and rNOE contributions and starts to reduce around 5 ppm, even though an appreciable component of about 4% asymmetry remains. While it is tempting to interpret this as MTC asymmetry, data will have to be acquired at larger offsets to confirm this.

Symmetric versus Asymmetric MTC based on experimental data

The limited experimental data in Figs. 6 and 7, together with more extensive studies by others (Hua et al., 2007; Swanson, 1998; Swanson et al., 2016) seem to indicate a substantial asymmetric MTC component on the order of a few percent (for B_1=1–3 μT), which can be concluded based on data at frequency offsets larger than 5 ppm. In addition, the asymmetry at frequency offsets in the proton spectral range (mobile molecules) is dominated by CEST and rNOE effects in mobile tissue components. Since many effects mix when performing an asymmetry analysis, the typical approach in the CEST world to name an effect after the predominant component at a certain frequency is not recommendable. So instead of APT MRI or gluCEST (glutamate CEST), one should use APT-weighted MRI and glu-weighted CEST, etc.

Simulating the contributions to the saturation transfer spectra *in vivo* is an enormous task. Any successful attempt would require to collect a wide range of experimental data covering a large range of saturation amplitudes and offset frequencies at multiple field strengths and apply a tissue model that consists of CEST, rNOE, and MTC pools and fit the corresponding Bloch equations. However, such an approach has severe limitations since it requires a priori information to define the number of exchanging pools, whereas in the complex tissue we may have too many degrees of freedom to determine all model parameters to describe exchange rates, pool sizes and their chemical shifts. One thing, however, that becomes apparent is that, within the proton spectral range, it is not easy to clearly separate magnetization transfer effects from mobile and semisolid tissue components. This is not surprising in view of the fact that all are currently measured using the same pulse sequences which cannot distinguish between dipole-dipole transfer and chemical exchange. The simple separation of CEST and MTC based on type of molecule (large vs. small) may be questionable as the tissue has constituents with a range of mobilities.

With respect to MTC, recent work (Xu et al., 2017) is starting to show some insight into semisolid tissue components, indicating both very fast and slower exchanging proton contributions to MTC. We

speculate that the fast ones may be from direct irradiation of OH groups, also suggested by Liepinsh and Otting (1996), or even bound water molecules that exchange rapidly to protons in free water, which would relate to frequencies close to the water resonance and thus a "symmetric component". The slower ones would be from relayed NOEs inside the aliphatic backbone, i.e., at frequency offsets for CH, CH_2, and

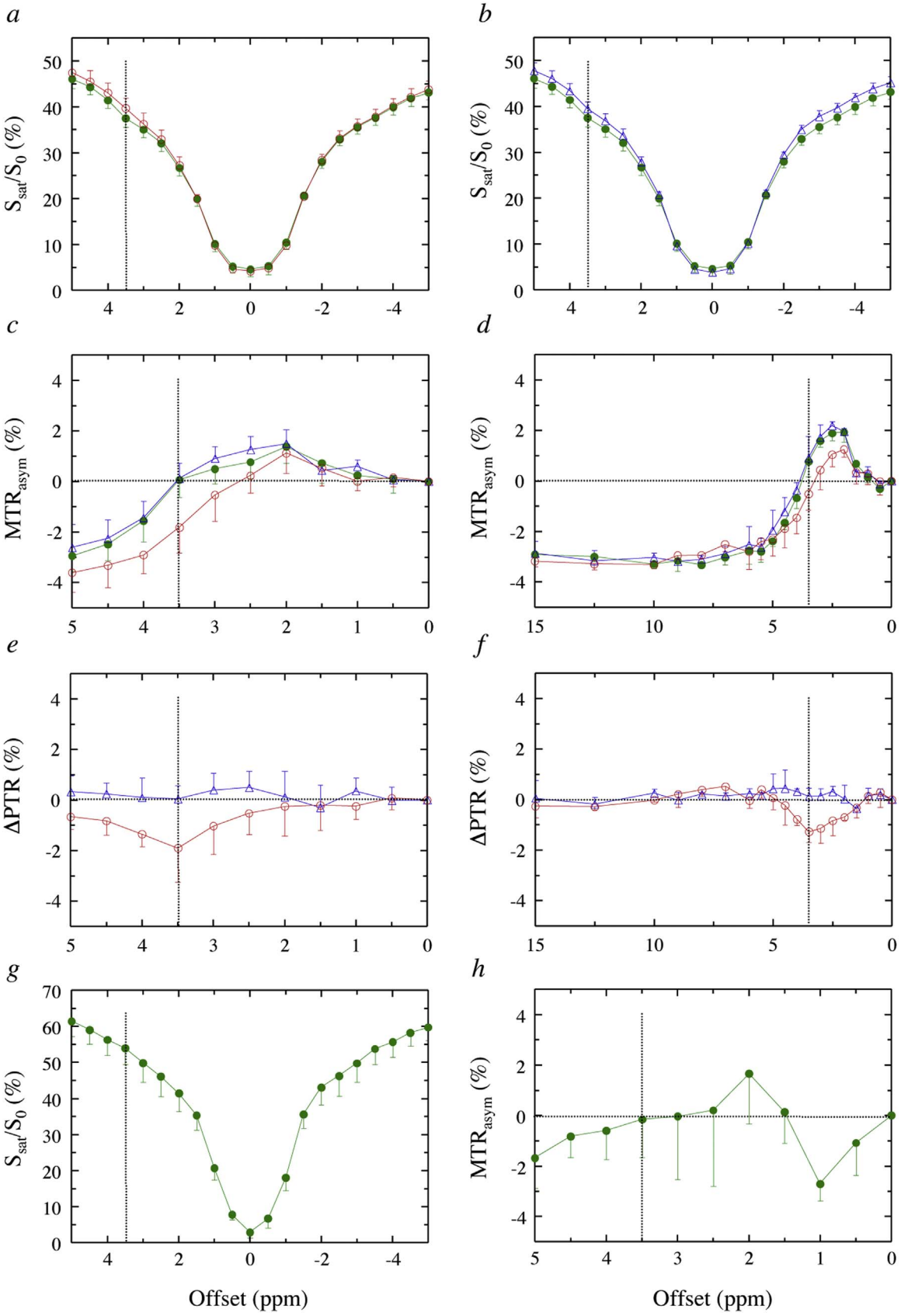

Fig. 6. Z-spectra and MTR_{asym} data for normocapnic (green), postmortem (cardiac arrest, red) and hypercapnic (blue) rat brain at 4.7 T. Five regions of interest covering the whole brain (fronto-parietal cortex, inferior colliculus, cerebellum) were chosen and averaged. In Z-spectra (a,b,g), signal attenuation is due mainly to the DE close to the water frequency and the MTC effect over the whole spectral range. MTR_{asym} data for brain (c,d) show a clear asymmetry in the proton spectral range (c) with the magnitude of the effects differing between postmortem and *in vivo*, explained in terms of a reduced pH postmortem reducing the CEST effects. The Z-spectrum asymmetry clearly extends well beyond the proton spectral range (d), indicating that it has to be due to asymmetry in the MTC. When choosing small areas with predominantly CSF (g,h) this asymmetry disappears due to the presence of just the DE. (e,f) When subtracting the MTR_{asym} spectra of normocapnia from those of postmortem and hypercapnia to get the difference in proton transfer ratio (PTR), the asymmetry at higher frequencies disappears and no effect remains for hypercapnia while the pH effect from cardiac arrest is visible only in the proton spectral range, with a maximum at 3.5 ppm. Saturation parameters: 400 Gaussian pulses (6.6 ms, delay 3.4 ms; total 4 s, average power 1.2 μT). Reproduced, with permission from Zhou et al. Nature Med. 9(8), 1085–1090 (2003). (For interpretation of the references to color in this figure legend, the reader is referred to the web version of this article.)

CH_3 groups and "asymmetric", the magnetization of which is relayed through the backbone and then transferred to exchangeable protons or direct through space to bound water. However, this will have to be proven still. Recent work by Lee et al. (2016) shows asymmetric MTC in normal white matter and symmetric MTC in brain tumors (known to have higher water content), which indicates dominance of different proton pools for these tissues. When performing MTC studies in other tissues, contributions will no doubt vary too.

Other analysis approaches for the Z-spectrum

While the standard and quickest way to analyze the Z-spectrum is by using the MTR_{asym}, it is founded on the assumptions that DE and MTC effects are symmetric and cancel out, and that signal at the same absolute frequency offset opposite from the water resonance has no saturation transfer contributions in addition to DE and MTC. While MTR_{asym} analysis has proven to be useful for many applications, it should be clear from the above that this assumption does not apply in practice, where rNOE effects of mobile proteins are clearly visible and asymmetric MTC effects may occur. As a consequence, investigators are exploring new analysis approaches in an attempt to separate out the actual signal components. Since the purpose of this paper is to provide insight into the field dependent features of MTC and CEST, we only provide a brief illustration of these other methods by using the simulated data set from Fig. 5 (Table 1) consisting of water, a symmetric MTC pool, four CEST pools (amide, glutamate, amine, and myo-inositol), and five relayed NOE pools. Spectra were simulated for two B_1 values at 7 T (Fig. 8a and b), either with all pools present (solid black lines), with only the DE and MTC pools (dashed black lines), or with DE, MTC, and one CEST or rNOE pool minus the DE-and-MTC-only spectrum. The latter was done to visualize the contributions from the individual CEST and rNOE pools at the bottom of the graphs. The amide (yellow-orange) component has a relatively small exchange rate with water (30 Hz); the guanidinium protons (red) a moderate rate (1100 Hz); the glutamate amine protons (green) and myo-inositol protons (blue), fast rates (5500 and 2000 Hz, respectively). This is reflected in the resulting spectral shape, which is symmetric about its resonance offset for the amide (3.5 ppm), while the glutamate and myo-inositol resonances are coalescing with that of water, leading to an asymmetric lineshape with an apparent maximum close to the water resonance and not at the appropriate resonance offsets of the NH_2 and OH resonance offsets (3 and 0.9 ppm, respectively). The guanidinium proton lineshape, shows an intermediate exchange effect, still resonant at 2 ppm. Importantly, since the glutamate resonance is close to that of the amide and the guanidinium protons, the broad coalesced glutamate-water lineshape overlaps with these, potentially confounding efforts to separate them, especially at higher B_1.

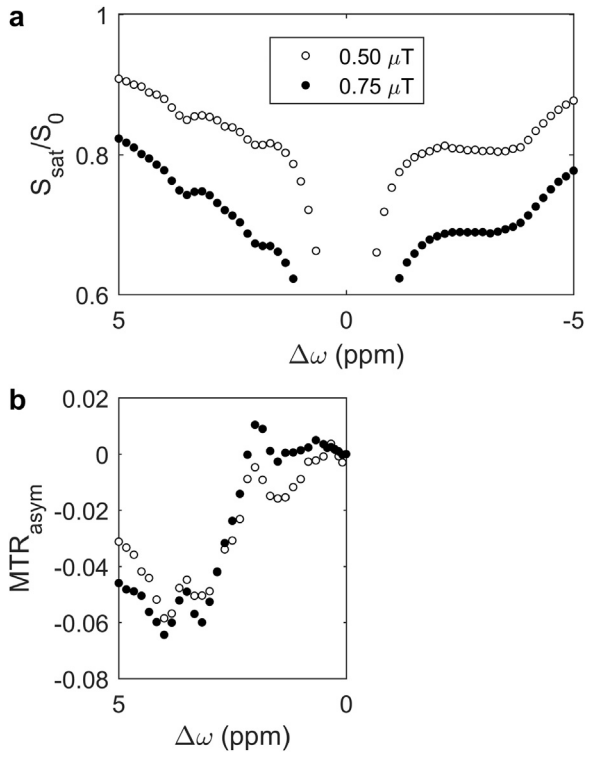

Fig. 7. Experimental (a) Z-spectra and (b) MTR_{asym} spectra for gray matter for mouse hippocampus at 7 T, using different B_1 values. Average of brain data for 10 mice. Unpublished results.

The general principle of the alternative methods is to fit the Z-spectrum by assuming a certain number of proton pools, including DE and symmetric MTC. In the simplest approach, applicable only at low B_1 where MTC is negligible at large offsets, the water resonance is fitted with a Lorentzian shape (using points close to its center and far off resonance) and subtracted out. This so-called Lorentzian difference (LD) approach allows the visualization of the slow exchanging amide and rNOE components (Jones et al., 2013). This is illustrated for the human brain in Fig. 9. However, even at this B_1 of 1 μT, an asymmetric broader MTC component is visible below the fine structure of the rNOE components. This seems to confirm that the asymmetric MTC component has a slow transfer rate, but this still has to be investigated in more detail. In more involved approaches, each proton pool is seen as separate and assigned a Lorentzian (L_i, which has amplitude, width, and height parameters). The labeled Z-spectral intensity, $Z_{lab}(\Delta\omega)$, is then composed of a constant baseline (Z_{base}, which would be 1 in a perfect world) plus n Lorentzian components (L_i):

$$Z_{lab}(\Delta\omega) = Z_{base} - \sum_{i=1}^{n} L_i(\Delta\omega) \quad (5)$$

While the MTC pool has been found to have a predominantly super-Lorentzian lineshape (Morrison et al., 1995), it has been approximated as a Lorentzian near its peak (Windschuh et al., 2015) or, due to its broad linewidth, assumed to be a constant attenuation across frequency offsets near 0 ppm (Desmond et al., 2014; Zhang et al., 2016a). The assumption of no interaction between the pools is not valid in general, but breaks down even more if the RF saturation pulse is too strong or when coalescence occurs in the fast exchange regime. Due to the phenomenological nature of this method it is difficult to interpret the physical basis of the model parameters. Figs. 8c and d show examples of attempted decomposition of the Z-spectra in Figs. 8a and b (solid black lines) into Lorentzian lineshapes by fitting to a multi-Lorentzian model and clearly demonstrate the problem with this oversimplified approach. In cases where CEST pool lineshapes have

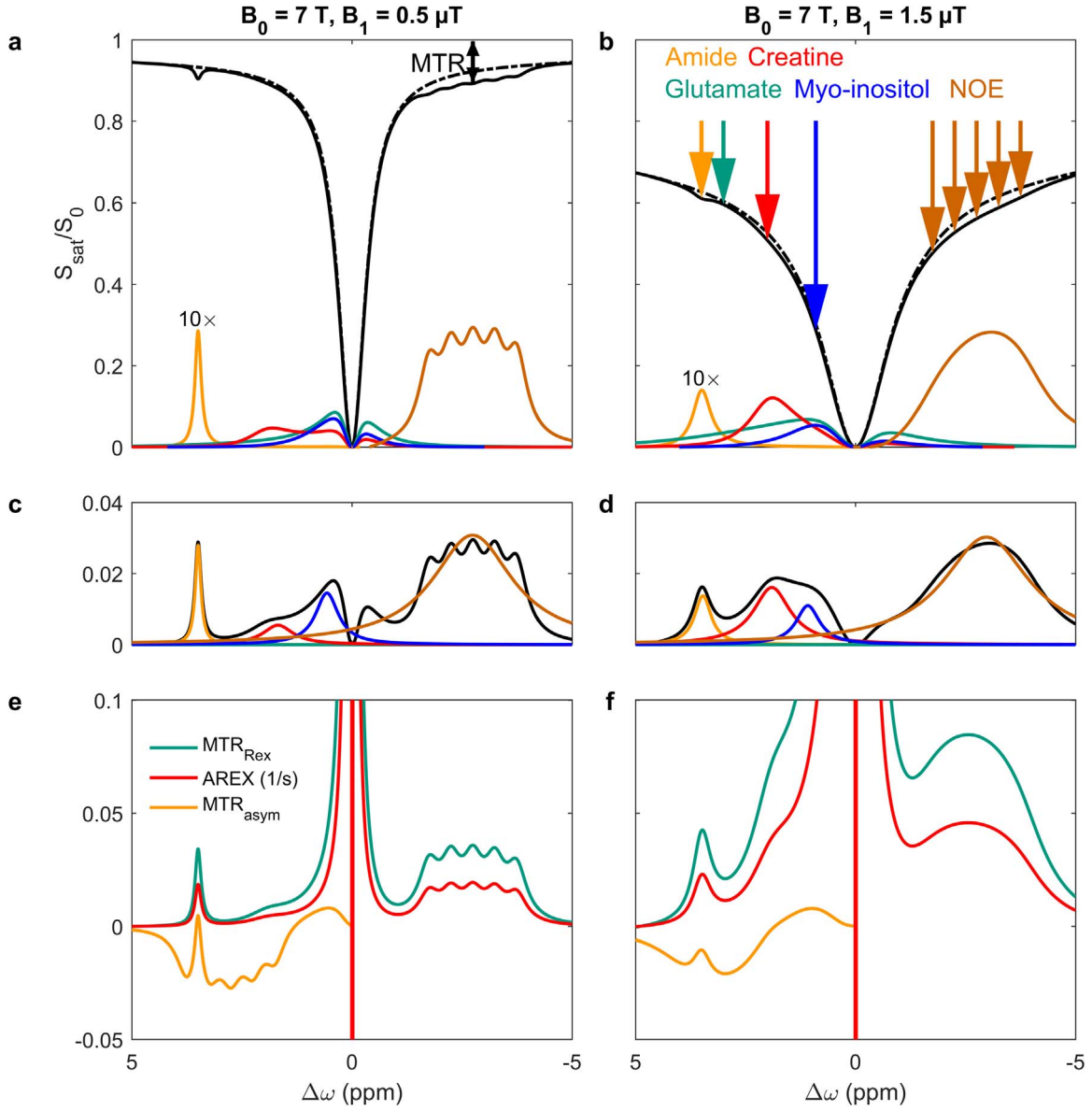

Fig. 8. Different types of spectral display at two saturation RF amplitudes B_1 based on simulations of gray matter for B_0=7 T in Fig. 5**(a,b)** Dashed black lines include DE and MTC. Solid black lines include DE, MTC, and CEST. Solid colored lines are spectra from DE, MTC, and single CEST pools subtracted from a spectrum with only DE and MTC in order to show contributions from individual pools. Note that the glutamate and myo-inositol proton contributions have their peak maxima shifted to 0 ppm because their high exchange rate merges their apparent peak positions and heights with those of water in a population-based averaging. The original offsets of the CEST components are indicated by arrows in (b). The double-sided arrow in (a) shows the magnetization transfer ratio (MTR) measure. (c,d) Lorentzian fits to the difference between the dashed and solid lines in a and b (black lines in c and d), respectively (colors as in b). (e,f) CEST metrics MTR_{Rex}, AREX, and MTR_{asym}. (For interpretation of the references to color in this figure legend, the reader is referred to the web version of this article.)

coalesced with that of water, the lineshape is no longer Lorentzian (see glutamate, myo-inositol and even creatine in Figs. 8a and b) and fitting will fail (Zhang et al., 2017a, 2017b). Note also that since the multi-Lorentzian model does not account for interaction between CEST pools and water, the sum of fitted Lorentzians will erroneously results in higher signal near 0 ppm where the tails of multiple Lorentzians overlap (not explicitly shown). The rNOE components are generally fitted using one component, which is also not realistic.

Despite the inaccuracy for assessing fast exchanging components, the Lorentzian fitting is gaining some popularity, especially in combination with inverse Z-spectral analysis (Zaiss et al., 2014). In this analysis, each component $Z_{lab,j}$ (Eq. 5) is combined with the baseline (reference value, $Z_{ref,j}(\Delta\omega) = Z_{base} - \sum_{i\neq j}^{n} L_i(\Delta\omega)$) at that frequency through inverse addition, which has theoretically been shown to provide a spillover (DE-) and MTC-corrected contrast for the exchange-dependent relaxation contribution, Rex, (Zaiss and Bachert, 2013b)

$$MTR_{Rex}(\Delta\omega) = \frac{1}{Z_{lab}} - \frac{1}{Z_{ref}}. \quad (6)$$

This analysis is sometimes expanded to include a theoretical correction for the effect of T_{1w} (Eq. (1)), the so-called water relaxation compensated CEST method, isolating the apparent exchange-dependent relaxation (AREX), presumably dependent only on $x_s \cdot k_{sw}$ when assuming a fully saturated component in the slow exchange regime:

$$AREX(\Delta\omega) = MTR_{Rex}(\Delta\omega)/T_{1w}. \quad (7)$$

Examples of these analyses can be seen in Fig. 8e–f. They work well for slow-exchanging amide and rNOE signals at low B_1, but become more difficult with increasing B_1 due to the division by small numbers close to the large remaining water signal.

An improvement over the Lorentzian approach is use of the Bloch

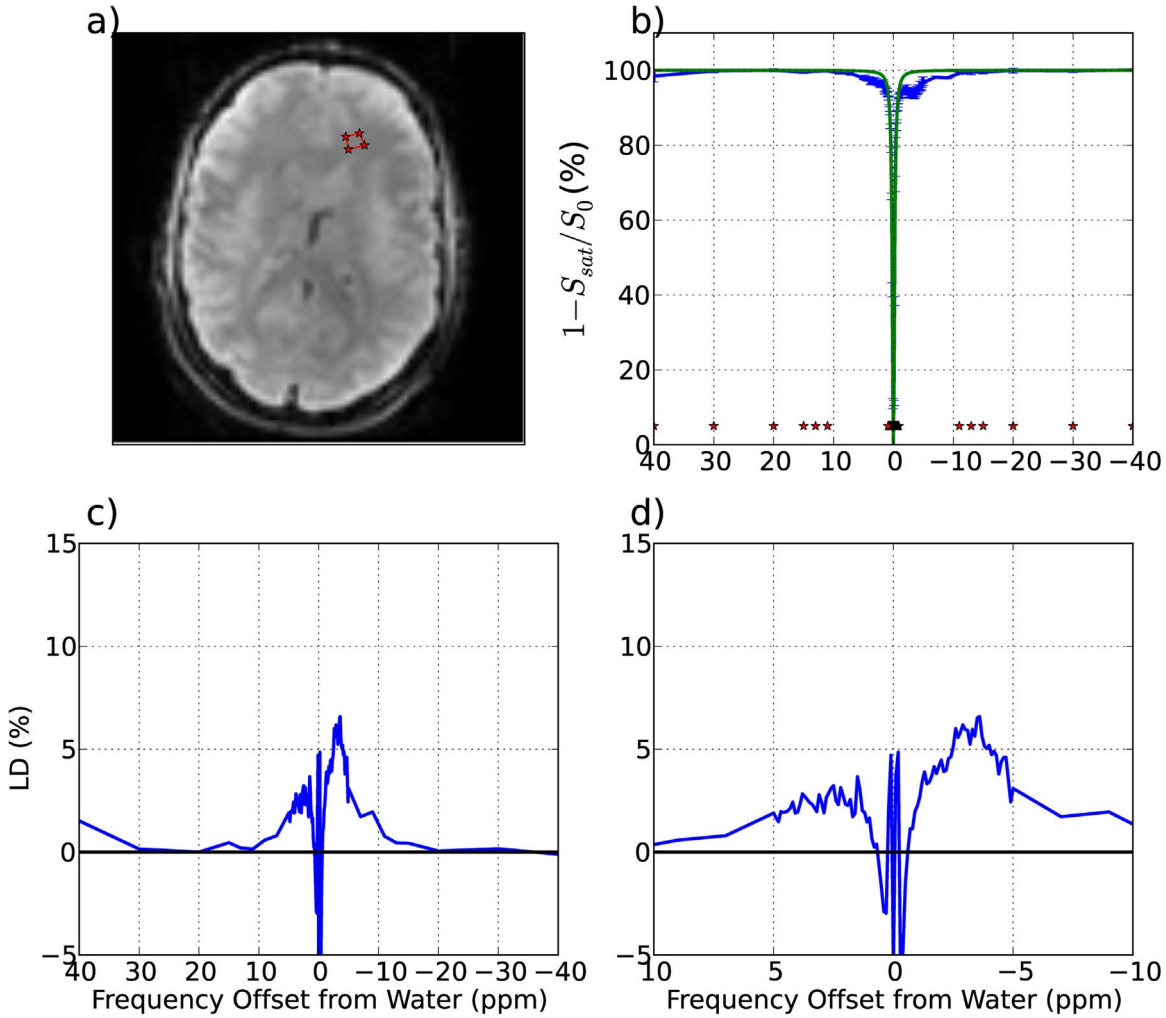

Fig. 9. Experimental human data at 7 T. (a) Axial unsaturated image and white matter ROI, **(b)** Z-spectrum and Lorentzian fit (green line) of the direct water saturation contribution based on fitting the frequency offsets shown as red stars for the ROI. **(c)** Lorentzian difference (LD) spectrum (40 to −40 ppm) for the ROI, defined as the difference between the Lorentzian fit and the acquired Z-spectrum. **(d)** LD spectrum zoomed in to 10 to −10 ppm. Data acquired using pulsed steady state acquisition (25 ms Sinc-Gauss pulse, B_1=1 μT, gradient echo detection TE/flip angle=1.72 ms/12°; whole brain acquisition 10.9 s per frequency). Notice the substantial MTC contribution and its asymmetry at 10 ppm as well as the fine structure due to multiple rNOE components for mobile macromolecules. Reproduced with permission from Jones et al. NeuroImage. 77:114-24 (2013). (For interpretation of the references to color in this figure legend, the reader is referred to the web version of this article.)

equations to fit Z-spectra in the rotating frame (Desmond and Stanisz, 2012; Heo et al., 2016b, 2016c; Lee et al., 2016) or the effective B_1 field frame (Zaiss et al., 2015a, 2015b). Further Z-spectra at powers sensitive to MTC can be acquired to constrain the MTC pool parameters. While the Bloch equations take into account exchange between the individual pools with water, they do not include exchange between the MTC and CEST pools and still assume only a limited number of pools. As well, the process of relayed NOE between coupled spins cannot be described by this classical approach and only be approximated as one or more individual pools. Although a powerful tool, Bloch equations are not without their problems. The most notorious one is a lack of sufficient observables allowing the separation of various parameters (such as exchange rate, proton fraction and T_2 of the CEST components). This is even visible in phantoms (Desmond and Stanisz, 2012) where CEST concentration is very high and control over experimental conditions is much better. For instance, when applying Bloch fitting to the experimental data for mouse hippocampus at 7 T (Fig. 7), the presence of very broad peaks centered at 3.5 ppm, 2 ppm, and −3.4 ppm might be interpreted as single amide, amine and rNOE pools, respectively. In this particular case the data may indicate only three exchanging CEST components, while we know from physiology and can see from Fig. 9 that more pools are present. Thus, although a good fit may be found, it may not be realistic and result in unphysical parameters such as very high concentrations and low T_2 relaxation times of the CEST components caused by multiple underlying components at each peak position.

Another very similar approach is to empirically remove just the combined baseline features from DE and MTC, the so-called extrapolated semisolid magnetization transfer reference (EMR) approach. Assumptions are made for the shape of this broad baseline (symmetric or asymmetric) and high-frequency-offset features in the Z-spectrum are used to Bloch fit DE and MTC, subtract them out, and subsequently analyze the remaining signal components (Heo et al., 2016b, 2016c; Lee et al., 2016). The resulting difference then simply represents contributions of the CEST and rNOE effects, dominated by amide, amine and aliphatic protons (e.g. see Fig. 8a,b). In this approach, the 3.5 ppm and −3.5 ppm components have been denominated as APT$^{\#}$ and NOE$^{\#}$. Depending on whether symmetric or asymmetric MTC is assumed, the resulting numbers and their MTR_{asym} may differ, with the asymmetric approach most likely being more correct. This approach has the convenient practical aspect of speed, but, similar to the MTR_{Rex} and AREX, except at very low powers for amides and rNOEs, the differences are not pure nor the component assignments accurate and resulting quantification will depend on the B_1 level used.

Finally, some investigators have used a three point analysis approach (Jin et al., 2013) to draw a baseline and to determine the

CEST (mainly APT, amine and rNOE) effects from simple subtraction, sometimes in combination with inverse Z-spectral analysis (Zaiss et al., 2014). Obviously, such analysis will have contaminating components, but may still be useful for studying pH effects or amide or guanidinium intensities, especially at lower B_1.

Z-spectral editing with pulse sequences

All of the above alternative analysis approaches use theoretical underpinnings regarding the system, especially that the DE and MTC dominated baseline and the individual CEST components can somehow be fitted out. The accuracy of the analysis will of course depend on the assumptions made and it is hard to prove that any components derived in such a manner are really "pure" or the analyses "unbiased", despite claims being made in that respect. It would thus be better if experimental approaches could be designed that can remove some of the contributing components to better visualize the species of interest. Fortunately, throughout its history, NMR has shown the ability for designing pulse sequences that can separate out spin systems based on their frequency offsets and different physical and timing properties, e.g. such as their chemical shift evolution, exchange transfer rates, and relaxation times in Table 1. Such sequences predominantly use excitation, which would not be useful for MTC studies, because of the short T_2 causing the spins to dephase and the pools to saturate. However, CEST MRI is about the mobile components that have a finite T_2, so the spin pools can be selectively excited and manipulated and this information transferred to the water signal where it shows up as signal loss. This field of editing for CEST components is still in its infancy, but currently several pulse sequences are already available, using either saturation difference (Lee et al., 2012; Narvainen et al., 2010; Scheidegger et al., 2011; Song et al., 2012, 2015; Vinogradov et al., 2012; Xu et al., 2014, 2016), excitation (Friedman et al., 2010; Lin et al., 2012; Xu et al., 2017, 2014; Yadav et al., 2012; Zu et al., 2012, 2013) or hybrid excitation-saturation (Friedman et al., 2015). The state of the art has been reviewed recently (van Zijl and Sehgal, 2016) and we refer the reader to that paper for study of the details. To illustrate the principles, we highlight a saturation-difference sequence that can remove the broad MTC background and most of the DE, the results of which can then be compared with some of the fitting analyses above.

The example chosen is one of the so-called variable-delay multi-pulse (VDMP) approaches (Xu et al., 2017, 2014), consisting of a series of excitation or saturation pulses (Fig. 10) separated by an inter-pulse delay time t_{mix}, in which the spin pools exchange information (they mix magnetization). While both slow- and fast-exchanging protons are labeled during the saturation pulses, their saturation buildup during t_{mix} differs appreciably. For fast-exchanging protons, the partially labeled spins already fully exchange with water protons during the RF pulse, and negligible additional transfer takes place during t_{mix}. As a consequence, the CEST signal decays with relaxation time constant T_{1w} (Fig. 10b). For slow-exchanging protons, the labeled spins take longer to transfer to water and this process continues during t_{mix}, causing the saturation of water to increase before starting to decay with T_{1w} (Fig. 10b). The buildup patterns for the VDMP method closely resemble the NOESY curves commonly measured in high-resolution NMR (Cavanagh et al., 2007). The difference in buildup patterns can be used to separate different spin pools by fitting the buildup curves. Alternatively, one of the components can be removed by subtracting signals acquired at two mixing times where its water saturation is equal. Fig. 10c–g shows an example of using such VDMP difference editing for suppressing the MTC pool in the human brain. It was empirically established that mixing times of 0 and 100ms have about the same VDMP signal for MTC (Fig. 10c). The MTC contrast that is clearly visible at t_{mix}=0 ms (Fig. 10d) disappears when subtracting these two images (Fig. 10e), allowing generation of VDMP difference images at 3.5 ppm (predominantly APT) and at -3.5 ppm (predominantly rNOE). Due to the long T_{1w}, most of the DE is also removed. Interestingly, this result shows larger APT in gray matter (GM) than in white matter (WM), but about equal rNOE. Assuming that the rNOE signals come predominantly from mobile macromolecules (MM) (van Zijl et al., 2003), this is a gratifying result because MRS data show the same effects of equivalency of MM concentrations in these two tissues (Snoussi et al., 2015). It is interesting to compare this result to MTR_{Rex} data by (Windschuh et al., 2015), also acquired at 7 T. Similarly, the amide image shows high intensity in GM, but the rNOE image is somewhat lower in GM. We tentatively attribute this to some contamination by MTC, similar to the data in Fig. 9, where the MM component sits on a broader MTC component.

It is important to note that the VDMP technique can in principle also be used for quantification of different MTC components when applying the on-resonance version (Xu et al., 2017), in which the semi-solid and mobile macromolecules and fast-exchanging protons are labeled efficiently by binomial pulses applied at the water resonance. Varying the mixing time is an accurate procedure controlled in MRI scanners, while the use of B_1-dependence in conventional quantitative MT (qMT) is sensitive to hardware conditions (power loss, B_1 inhomogeneity, specific absorption rate (SAR) and amplifier restrictions).

High field saturation transfer experiments – advantages and issues

It should be clear from the previous sections that water Z-spectra contain a mix of information from many components, the contributions of which will vary substantially depending on the experimental parameters, such as pulse sequence used (RF pulse shape, length and interpulse timing), the RF field strength B_1, and the magnetic field strength B_0. Fig. 11 shows simulations of how these contributions vary with B_0 and B_1 for the simple situation of continuous saturation and the example of 4 CEST pools (main brain contributions of protein amides, creatine, glutamate, myo-inositol), 5 rNOE-pools, symmetric MTC, and DE used above in Figs. 4 and 8. These simulations are noise-free, but the usual increase of SNR with B_0 (increased polarization) will benefit these experiments at higher field.

A quick glance at the Z-spectra in Fig. 11 shows that, similar to MRS, the use of high field scanners has the clear advantage of improving the frequency separation between the resonances of the spin pools. However, compared to MRS, where predominantly aliphatic resonances are studied, the use of higher field is even more important for CEST because increasing B_0 facilitates a progression towards the slow-exchange condition and reduced interference of direct water saturation. While the amide protons and rNOEs are in the slow exchange regime for all three fields, the other CEST pools simulated are not. For example, at low B_1 (0.5 μT, top row in Fig. 11), the creatine resonance (assumed k_{sw} of 1100 Hz) is in the intermediate exchange regime, with an indistinguishable resonance at 3 T that only becomes visible at 7 T and higher. Glutamate and myo-inositol remain in the intermediate-to-fast regime and coalesce with water even at the higher fields, but still cause an asymmetry in the Z-spectrum that may be detectable under favorable conditions. At low B_1 (0.5–1 μT), in our example, the contributions to the Z-spectrum are therefore dominated by the slow-exchanging amides and rNOEs, and at higher B_0 the guanidinium protons from creatine. The fine structure of the rNOEs may become visible at low B_1, which was found in recent pulsed steady state data (Jones et al., 2013) (Fig. 9).

It should be clear from these simulations that it will be hard to detect fast-exchanging OH and amine groups at low B_0. For instance, the glutamate protons cannot be distinguished from creatine at 3 T and OH groups are mixed with glutamate and creatine protons even at the higher field. The current simulations are for continuous saturation, and in view of the results, it seems unlikely that glutamate or myo-inositol detection in brain can be done well at 3 T without advanced editing. At

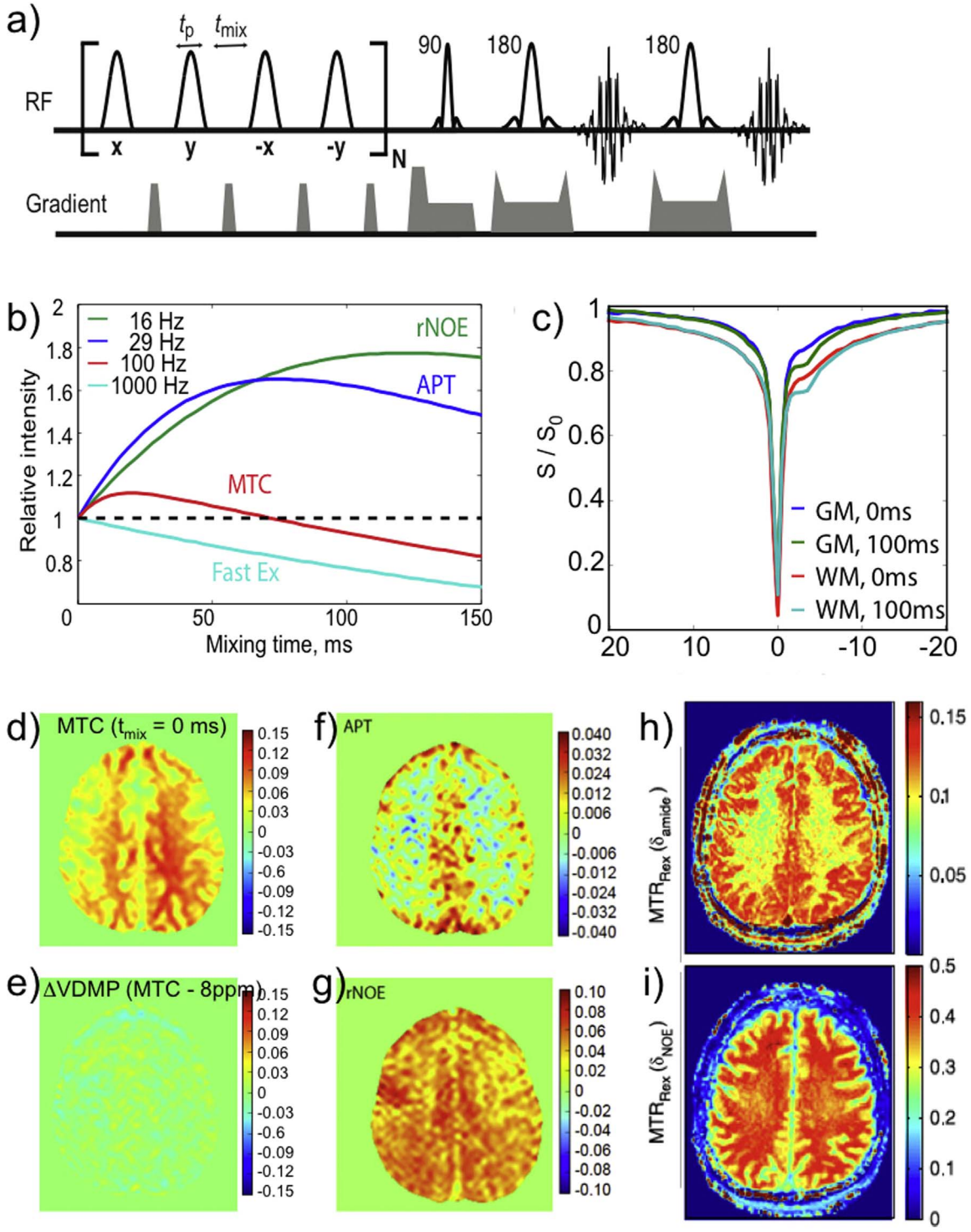

Fig. 10. Variable delay multi pulse (VDMP) CEST editing and relaxation compensated CEST imaging in human brain at 7 T. (a) Multi-echo MRI pulse sequence with VDMP saturation preparation train of Gaussian 180° pulses (width t_p, inter pulse delay t_{mix}, crushers to suppress residual transverse magnetization). Every set of 4 pulses is cycled using the "CYCLically Ordered Phase Sequence" (CYCLOPS) approach, i.e. 90° steps (x, y, -x, -y) to complete a cycle. **(b)** Simulation of saturation buildup as a function of t_{mix} for four typical spin pool transfer rates: rNOE (16 Hz), APT (29 Hz), MTC (60 Hz), and fast exchange (1000 Hz). All intensities normalized to the first data point (t_{mix}=0 ms) to make curves independent of the concentration of exchanging protons. **(c)** In vivo Z-spectra of human brain at t_{mix}=0 ms and at t_{mix}=100 ms (optimized for compensating for MTC). **(d-f)** VDMP difference maps for MTC at 8 ppm **(d)**, APT **(e)** and rNOE **(f). (g-h)** MTR_{Rex} images in another volunteer acquired at the APT and rNOE frequencies. Reproduced, with permission from: **(a)** Xu J. et al. MRM 71:1798-1812 (2014); **(b-f)** Xu J. et al. 75:88-96 (2016) MRM; **(g,h)** Windschuh et al. NMR Biomed. 2015; 28: 529–537.

7 T and B_1=4 μT, for the current limited number of CEST pools in our simulation, glutamate protons are the main contribution at 3 ppm (> 50%), but the effect is about 0.4%, a contribution that increases at 11.7 T. Thus, in line with the original report for gluCEST (Cai et al., 2012), such detection should in principle be possible but the mentioned caveat of limited pools in the simulation should be kept in mind. However, as a more positive caveat, experiments use limited saturation time (500–1000 ms) instead of steady state continuous irradiation and the slow-exchange MTC effects will reduce and fast exchanging protons may become better visible. Detection of myo-inositol seems proble-

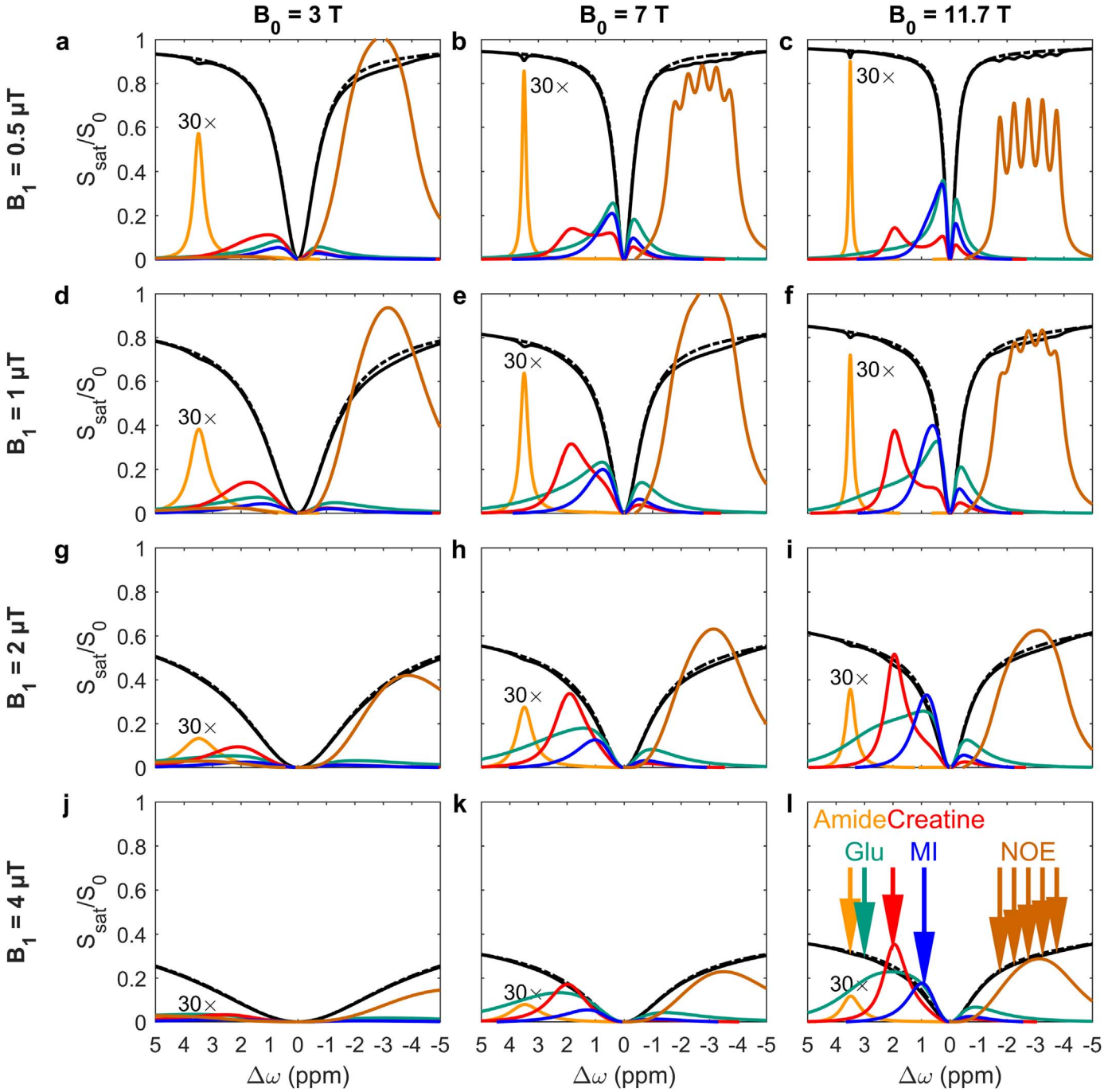

Fig. 11. Simulations of the B_0 dependence of Z-spectra of gray matter using continuous saturation at different B_1 levels. Parameters used are listed in Table 1 and Figs. 4 and 5. Notice the coalescence of the fast exchanging glutamate amine and myo-inositol hydroxyl resonances with the water resonance and the improving appearance of the creatine guanidinium protons at higher field due to moving towards the slow exchange regime.

matic at any field due to its coalescence with water and overlap with glutamate. Notice that such compounds can be detected in phantoms in one-component solution due to the large asymmetry for the intermediate exchange case, but most likely not cleanly in mixtures with each other, unless with some use of editing. Thus, care has to be taken to claim detection of any of these compounds in tissue, unless either a physiological paradigm or a contrast agent can be used (e.g. glucose, (Chan et al., 2012; Nasrallah et al., 2013; Walker-Samuel et al., 2013; Xu et al., 2015a, 2015b) to specifically alter the concentration of one of these, allowing difference imaging for its visualization. Similar issues will exist for other organs, with the visibility depending on the presence of other compounds (e.g. glycogen and creatine in the muscle) and the use of certain analysis techniques. Finally, since power deposition goes with the square of the field strength, SAR and amplifier performance will become an issue at higher B_0 and make the use of continuous wave (CW) saturation at high B_1 difficult. On the other hand, SAR is inversely proportional to the coil diameter and the use of smaller, more local, transmit coils or parallel transmission may alleviate this problem in part. The B_0 correction for Z-spectra becomes more important at high field, but since such corrections are done on a voxel-by-voxel basis, this should not be an issue.

While higher field clearly benefits CEST MRI in terms of resonance dispersion, this advantage is not relevant for MTC data, with the microsecond T_2 causing a broad signal. However, it is important to comment on effects that may occur when using higher fields. In the 1.5 T literature, an irradiation offset of 1000 or 1500 Hz was recom-

mended, which corresponds to about 16–24 ppm, and thus well outside the spectral range. However, the lower limit reduces to about 8 ppm and 4 ppm at 3 T and 7 T, thus moving into the proton spectral range and causing contamination of MTC with CEST or rNOE components, especially at negative frequency with respect to water. Thus the offset recommendation should probably be in ppm and for positive frequency. In addition, experimental data such as in Fig. 6 show a clear asymmetry in MTC-based saturation even at higher offsets. This is in addition to the effect size depending on the pulse sequence parameters. Thus, when designing clinical trials for MTC, a single frequency offset in ppm (> 10 ppm) at one side of the water signal is recommended, together with exactly the same pulse sequence in terms of RF pulse shape, length, number of pulses, interpulse delay, and even imaging sequence as any RF components in the imaging part may contribute to the MTC. More quantitative MTC (qMTC), independent of the imaging sequence, would be possible by varying B_1 or timing inside the saturation preparation, which is the topic in qMTC (Gochberg and Gore, 2003; Harrison et al., 1995; Sled and Pike, 2001; Stanisz et al., 1999). Methods are also being developed to separate out symmetric and asymmetric and fast and slow MTC components (Xu et al., 2017). Finally, recent studies at higher field have shown contrast between different gray matter regions depending on their iron content. This is well possible as the iron will affect the magnetic susceptibility of the tissue and thus shift the line shape center frequency. This may be useful for studying iron content (Smith et al., 2006), but can be avoided by centering the water frequency in each voxel using one of the methods for B_0 correction mentioned above.

Using the endogenous Z-spectrum for the study of disease

It should be clear from the above considerations that the in vivo Z-spectrum is a complex acquisition-parameter-dependent observable, the interpretation of which has to be done carefully to avoid overstated or even erroneous conclusions. In the end, validation of any CEST or MTC approach has to come from biochemical verification and from reproducibility studies between multiple laboratories using equivalent parameter settings. Despite many shortcomings for each of the above described analysis approaches, several of them still provide useful information for assessing features of the CEST spectrum and even show potential for making some clinical inferences. However, it has to be realized that their suitability is related to the particular application. For instance MTR_{asym} analysis, while used for most applications until now, clearly is the "dirtiest" approach when it comes to mixing of signals (CEST, symmetric MTC, rNOE). However, such an analysis has lead to several successful clinical applications, while the interpretative value of other more advanced approaches is, to a large extent, still to be proven in situ.

The best example of successful use of MTR_{asym} analysis is at the amide proton frequency of 3.5 ppm using so-called APT-weighted MRI, which allows the clear detection of malignant brain tumors (Jones et al., 2006; Salhotra et al., 2008; Wen et al., 2010; Zhou et al., 2008, 2003a) and even the separation of recurrent tumors from treatment necrosis effects (Zhou et al., 2011). This potential is supported by clear results from multiple institutions around the world both in experimental models and humans using multiple scanner types (Jiang et al., 2016c; Ma et al., 2016; Park et al., 2015a; Park et al., 2015b; Sagiyama et al., 2014; Sakata et al., 2015; Togao et al., 2014; Wen et al., 2010; Zhao et al., 2013; Zhou et al., 2013) and is being confirmed by biopsy studies (Jiang et al., 2016a, 2016b). The success of this approach is based on a coincidental symbiotic effect of mixing the rNOE, APT and asymmetric MTC contributions. This symbiosis remains intact when removing the DE and symmetric MTC components using the above-mentioned symmetric EMR approach (Heo et al., 2016b, 2016c), and measuring the remaining $APT^{\#}$ effect at the amide proton frequency. An important caveat to this research (and most CEST research) is that the terminology "APT or APTw MRI" is vague and could include the use of a variety of pulse sequences and data analysis approaches that can produce conflicting outcomes between sites. This has also led to the phenomenon of criticism between groups based on claims that one approach is better (more unbiased or accurate) than that of another, based either on theoretical predictions or phantom data. This is unfortunate considering the complexity of the data and especially in view of the fact that most groups have used greatly different pulse sequence parameters in terms of pulse number, length, B_1 and spacing. Interestingly, this separating out of some of the components with other pulse sequences and analysis methods appears to in some cases remove the "high-grade tumor" specificity. For instance, when using the AREX or MTR_{Rex} analysis after Lorentzian background fitting for "purifying" the amide proton transfer effect, the results were no longer conclusive at the amide proton frequency (Zaiss et al., 2015a). When using these latter approaches, therefore, drawing of clinical inferences related to tumor grade and treatment effect versus recurrent tumor no longer seems possible as the information content has changed. However, they may have potential for other analyses, e.g. highlighting areas of blood brain barrier breakdown similar to contrast enhanced MRI (Zaiss et al., 2015a). Similar controversy for tumor analysis has been found when using shorter RF pulses and higher B_1 than in the original APT-weighted literature (Desmond et al., 2014; Scheidegger et al., 2014). Thus for this approach with important potential to become standard in the clinic, it will be essential for the scanner companies to automate it with the appropriate B_1 and t_{sat} settings and analysis approaches. For instance, while APT-weighted analysis has clearly showed the potential for mapping pH changes during ischemia (Sun et al., 2007; Zhou et al., 2003b; Zhou and van Zijl, 2011), purer APT signals such as obtained by the EMR approach are more suitable to study pH effects during ischemia, because they avoid mixing of rNOEs and CEST effects (Heo et al., in press; Leigh et al., 2017), both of which are pH dependent (Jones et al., 2013).

The second most studied resonance with high abundance in the Z-spectrum is that of the guanidinium proton pool, mainly originating from Cr, PCr and some protein/peptide side chains. As Cr has the highest exchange rate (Goerke et al., 2014; Haris et al., 2012), about 6–10 times that of PCr, it is known to be the predominant contributor under typical in vivo conditions, especially in the brain where the concentrations of Cr and PCr are comparable in magnitude (Duarte et al., 2012) and the muscle (myocardium and skeletal muscle), where the Cr concentration typically is 40–80 percent higher than that of PCr (Bottomley, 2016, 1996, 1997). Because of the intermediate range exchange rate of Cr, the guanidinium resonance is partially collapsed with water at lower field, while it can be distinguished on the broad background at sufficiently high field (Fig. 11). Early work has focused on muscle, both skeletal and cardiac (Haris et al., 2014; Kogan et al., 2014a, 2014b). Again the MTR_{asym} ratio was used (called CrCEST or CrEST), sometimes with negative frequency offset reference instead of S_0. However, similar to APTw MRI, this approach results in mixing in of the rNOEs, in this case of for instance glycogen. Also, even when not using the MTR_{asym} ratio and even if DE and MTC could be removed with for instance Bloch fitting, there is mixing in of the broad coalesced signals of the OH protons of glycogen over the same frequency range (van Zijl et al., 2007). However, such arguments are no longer very relevant when one is studying either changes during a creatine-specific paradigm or comparing healthy with diseased tissue. Similar to APTw MRI, as long as a change is measured that is reproducible for a certain paradigm or disease, there may be clinical value, even if the interpretation is not totally clean. Using plantar flexion exercise in calf muscle as a paradigm, clear increases in the guanidinium signals could be found using high-resolution CrCEST MRI at 7 Tesla (Kogan et al., 2014a), in line with expectations of increasing Cr concentration. In addition, the muscle groups selectively involved in this type of exercise were highlighted in the difference images. While quantification of the effects in terms of pure Cr and quantification of concentrations is difficult due to the above arguments and the changing pH affecting the

Cr CEST signal, this simple approach has potential for many important in vivo applications involving energetics in many organs. One example of that was application of CrCEST to cardiac infarction, where a reduction in Cr was found instead of an increase, assigned to being possibly due to reduced pH and reduction in Cr after long periods of infarction (Haris et al., 2014). Overall, this muscle creatine work has great potential, but the confounding factors of changes in glycogen, pH and T_2 (Price and Gore, 1998) have to be accounted for in future work. With respect to other applications for Cr, recent work has shown potential to differentiate tumors from healthy tissue due to a lack of Cr in the tumor or reduced pH (Cai et al., 2015, 2017; Chan et al., 2016).

Another metabolite for which MTR_{asym} analysis has shown potential for brain (Cai et al., 2012; Cai et al., 2013; Singh et al., 2013) and spinal cord (Kogan et al., 2013) applications is glutamate (Glu). Despite this being a coalesced resonance even at fields as high as 11.7 T (Fig. 11), and the consequential overlap with other coalesced resonances from GABA, glutamine (Gln), and taurine (Tau), Reddy and coworkers (Cai et al., 2012, 2013; Singh et al., 2013) have reported that, under the right B_1 and B_0 conditions, Glu and changes in its concentration can be detected. This GluCEST approach has shown potential in several diseases. For instance, a 20 – 25% loss in MTR_{asym} at 3ppm was found for the hippocampus going from wild type to APPPS1 mice, a transgenic Alzheimer's disease model (Crescenzi et al., 2017, 2014; Haris et al., 2013a), which correlated with MRS data in the same mice while MTC contributions could be ruled out. Another nice demonstration of gluCEST is in a “Parkinsonian-type” mouse model where dopamine neuron deficiency was induced in the substantia nigra leading to astrogliosis and glutamate increase in the striatum (Bagga et al., 2016). GluCEST signal increases were confirmed by immunohistochemistry and MRS. Glutamate reductions were also reported in a mouse model of Huntington's Disease (Pepin et al., 2016), but here the results seem more complicated to interpret as large reductions in taurine (Tau) occurred, which also has a coalesced line shape over a similar frequency range as glutamate. Humans have lower Tau concentrations, so this may provide a lucky situation for applying such studies in the clinic. Overall, it is again a fortunate coincidence that at B_1 values above 4 μT at 7 T and 2 μT at 11.7 T, the Glu component is quite clean at 3 ppm as shown in Fig. 11. While these simulations do not take into account other amine containing compounds such as GABA, Gln and Tau, the detection of Glu in humans is favored due to its large in vivo concentration compared to these other metabolites. Therefore, glutamate changes should be well detectable although some contamination by other components is hard to rule out. But it has to be kept in mind that the clinic only requires a measurable reproducible effect that can be validated with other measures and, similar to APTw MRI, this may apply to several GluCEST applications. Recent impressive results using GluCEST to lateralize seizure foci in a small group of patients with non-lesional temporal lobe epilepsy (Davis et al., 2015) confirms this potential. Interestingly, while all of the above-mentioned studies used MTR_{asym} analysis for GluCEST, the simulated spectra in Fig. 11 indicate that it may be better to just use B_0-corrected Z-spectra, preferably with removal of the dominating MTC and DE components using Bloch equation fitting.

Finally, there have been reports of the ability of MTR_{asym} analysis at 0.6 ppm offset to detect myoinositol (MI) in healthy brain (Haris et al., 2011) and 50% changes in MI in AD (Haris et al., 2013b). Looking at Fig. 11, this should be quite complicated due to overlap with all coalesced signals, especially glutamate. However, myoinositol has a very high concentration (7.5 mM, corresponding to 45 mM OH protons), which may allow it detection, and the potential of this approach has to be proven in future detailed studies.

Overall, applications of conventional CEST have focused mainly on the use of MTR_{asym} analysis, with some good results especially for APTw MRI and GluCEST. Overall, removal of the dominating background signals from DE and MTC using such an asymmetry analysis has paid off. Similarly the use of Bloch fitting is showing potential for the same purpose, for instance for the use of APT in stroke imaging. This latter may be the best approach to combine with the *AREX* and MTR_{Rex} approaches. The use of simple Lorentzian fitting, either for the background signals or the remaining spectral components (many of them with coalescing lineshapes), seems to have too many pitfalls. However, much more work is needed to establish quantitative approaches for precise measurement or editing of pure metabolite effects and this may have to be done differently for different metabolites or even for the same metabolite at different field strength depending on the exchange regime. For reproducible application between laboratories and clinics, the scanner manufacturers will ultimately be needed to provide the optimum settings for each application as determined from basic research.

Conclusions and perspective

While MTC is a mature field with utility in several clinical applications, CEST imaging is a burgeoning young field that has given rise to new enthusiasm regarding the detection of millimolar metabolites and contrast agents using MRI instead of MRS. Similar to MRS, it can be expected that the use of high magnetic fields will strongly facilitate the CEST research endeavors and, through the availability of increased chemical shift dispersion and the use of advanced editing pulse sequences, allow detection of specific metabolites and agents. However, the above overview should also make clear that there are many caveats to overcome and that the taking of a simplified view for the detection of certain compounds from phantom results and the naming of a method after that will often be an oversimplification. For instance, common practice in the CEST literature has been to perform MTR_{asym} analysis in single-component physiological phantoms (buffer, pH ~7–7.3, T=37 °C) and naming the method after that (glycoCEST, gagCEST, gluCEST, MICEST, CrCEST, etc.). While, under favorable experimental conditions of an optimized pulse sequence and B_1, the intended component may dominate at a certain frequency, it is unlikely to be pure *in vivo* nor its detection unbiased or accurate. As such, it would be recommendable to call all approaches “weighted”, similar to that of other imaging methods. Fortunately, this is becoming recognized and at least the APT literature is moving to the terminology “APT-weighted”, which is definitely more applicable in view of the mixing of amide proton, asymmetric MTC and rNOE signals. Substitution of MTR_{asym} analysis by background removal methods based on Bloch fitting of the DE and MTC components improves the detection of some “purer” components, some of which can then be fit with Lorentzian analysis, but obviously not the fast-exchanging protons. Despite being theoretically sound, the use of inverse Z-spectral analysis for multi-components tissue analysis will also depend on the success of these background removal approaches and be complicated by spectral coalescence.

In conclusion, the CEST field has opened up great opportunities for the detection of millimolar agents and metabolites using actual MRI. However, due to the complexity of the *in vivo* tissue Z-spectrum, care has to be taken not to over-interpret the data. From the above, It should be clear that the optimum pulse sequence and B_1 need to be determined for each individual application and that detection of certain compounds is not feasible with CW saturation approaches, especially fast-exchanging protons at low B_0. The investigators in this CEST field thus have the task of optimizing the technologies and standardizing them in order to provide clinicians with successful technologies that can be reproduced between different MRI systems and different hospitals, an effort that will in many instances be facilitated by the use of higher magnetic fields. Our cautious prediction therefore is that many of the issues discussed in this contemporary review will be resolved in the coming decade.

References

Aime, S., Castelli, D.D., Crich, S.G., Gianolio, E., Terreno, E., 2009. Pushing the sensitivity envelope of lanthanide-based magnetic resonance imaging (MRI) contrast agents for molecular imaging applications. Acc. Chem. Res. 42, 822–831.

Bagga, P., Crescenzi, R., Krishnamoorthy, G., Verma, G., Nanga, R.P., Reddy, D., Greenberg, J., Detre, J.A., Hariharan, H., Reddy, R., 2016. Mapping the alterations in glutamate with GluCEST MRI in a mouse model of dopamine deficiency. J. Neurochem. 139, 432–439.

Balaban, R.S., Ceckler, T.L., 1992. Magnetization transfer contrast in magnetic resonance imaging. Magn. Reson Q 8, 116–137.

Behar, K.L., Rothman, D.L., Spencer, D.D., Petroff, O.A., 1994. Analysis of macromolecule resonances in 1H NMR spectra of human brain. Magn. ResonMed. 32, 294–302.

Bottomley, P.A., 2016. MRS studies of creatine kinase metabolism in human heart. eMagRes 5,
1183–1202, (DOI 1110.1002/9780470034590.emrstm9780470031488).

Bottomley, P.A., Atalar, E., Weiss, R.G., 1996. Human cardiac high-energy phosphate metabolite concentrations by 1D-resolved NMR spectroscopy. Magn. Reson Med 35, 664–670.

Bottomley, P.A., Foster, T.H., Argersinger, R.E., Pfeifer, L.M., 1984. A review of normal tissue hydrogen NMR relaxation times and relaxation mechanisms from 1 to 100 MHz: dependence on tissue type, NMR frequency, temperature, species, excision, and age. Med. Phys. 11, 425–448.

Bottomley, P.A., Lee, Y., Weiss, R.G., 1997. Total creatine in muscle: imaging and quantification with proton MR spectroscopy. Radiology 204, 403–410.

Bryant, R.G., 1996. The dynamics of water-protein interactions. Annu. Rev. Biophys. Biomol. Struct. 25, 29–53.

Cai, K., Haris, M., Singh, A., Kogan, F., Greenberg, J.H., Hariharan, H., Detre, J.A., Reddy, R., 2012. Magnetic resonance imaging of glutamate. Nat. Med. 18, 302–306.

Cai, K., Singh, A., Poptani, H., Li, W., Yang, S., Lu, Y., Hariharan, H., Zhou, X.J., Reddy, R., 2015. CEST signal at 2 ppm (CEST@2 ppm) from Z-spectral fitting correlates with creatine distribution in brain tumor. NMR Biomed. 28, 1–8.

Cai, K., Singh, A., Roalf, D.R., Nanga, R.P., Haris, M., Hariharan, H., Gur, R., Reddy, R., 2013. Mapping glutamate in subcortical brain structures using high-resolution GluCEST MRI. NMR Biomed. 26, 1278–1284.

Cai, K., Tain, R.W., Zhou, X.J., Damen, F.C., Scotti, A.M., Hariharan, H., Poptani, H., Reddy, R., 2017. Creatine CEST MRI for differentiating gliomas with different degrees of aggressiveness. Mol. Imaging Biol. 19, 225–232.

Cavanagh, J., Fairbrother, W.J., Palmer, A.G., Skelton, N.J., Rance, M., 2007. Protein NMR Spectroscopy Principles and Practice. Elsevier Academic Press, Burlington, MA, USA.

Chan, K.W., Jiang, L., Cheng, M., Wijnen, J.P., Liu, G., Huang, P., van Zijl, P.C., McMahon, M.T., Glunde, K., 2016. CEST-MRI detects metabolite levels altered by breast cancer cell aggressiveness and chemotherapy response. NMR Biomed. 29, 806–816.

Chan, K.W., McMahon, M.T., Kato, Y., Liu, G., Bulte, J.W., Bhujwalla, Z.M., Artemov, D., van Zijl, P.C., 2012. Natural D-glucose as a biodegradable MRI contrast agent for detecting cancer. Magn. Reson. Med. 68, 1764–1773.

Crescenzi, R., DeBrosse, C., Nanga, R.P., Byrne, M.D., Krishnamoorthy, G., D'Aquilla, K., Nath, H., Morales, K.H., Iba, M., Hariharan, H., Lee, V.M., Detre, J.A., Reddy, R., 2017. Longitudinal imaging reveals subhippocampal dynamics in glutamate levels associated with histopathologic events in a mouse model of tauopathy and healthy mice. Hippocampus 27, 285–302.

Crescenzi, R., DeBrosse, C., Nanga, R.P., Reddy, S., Haris, M., Hariharan, H., Iba, M., Lee, V.M., Detre, J.A., Borthakur, A., Reddy, R., 2014. In vivo measurement of glutamate loss is associated with synapse loss in a mouse model of tauopathy. Neuroimage 101, 185–192.

Davis, K.A., Nanga, R.P., Das, S., Chen, S.H., Hadar, P.N., Pollard, J.R., Lucas, T.H., Shinohara, R.T., Litt, B., Hariharan, H., Elliott, M.A., Detre, J.A., Reddy, R., 2015. Glutamate imaging (GluCEST) lateralizes epileptic foci in nonlesional temporal lobe epilepsy. Sci. Transl. Med 7, 309ra161.

Desmond, K.L., Moosvi, F., Stanisz, G.J., 2014. Mapping of amide, amine, and aliphatic peaks in the CEST spectra of murine xenografts at 7 T. Magn. Reson. Med. 71, 1841–1853.

Desmond, K.L., Stanisz, G.J., 2012. Understanding quantitative pulsed CEST in the presence of MT. Magn. Reson. Med. 67, 979–990.

Duarte, J.M., Lei, H., Mlynarik, V., Gruetter, R., 2012. The neurochemical profile quantified by in vivo 1H NMR spectroscopy. Neuroimage 61, 342–362.

Edzes, H.T., Samulski, E.T., 1977. Cross relaxation and spin diffusion in the proton NMR or hydrated collagen. Nature 265, 521–523.

Forsen, S., Hoffman, R.A., 1963. Study of moderately rapid chemical exchange reactions by means of nuclear magnetic double resonance. J. Chem. Phys. 39, 2892–2901.

Friedman, J.I., McMahon, M.T., Stivers, J.T., Van Zijl, P.C., 2010. Indirect detection of labile solute proton spectra via the water signal using frequency-labeled exchange (FLEX) transfer. J Am. Chem. Soc. 132, 1813–1815.

Friedman, J.I., Xia, D., Regatte, R.R., Jerschow, A., 2015. Transfer rate edited experiment for the selective detection of chemical exchange via saturation transfer (TRE-CEST). J. Magn. Reson. 256, 43–51.

Gochberg, D.F., Gore, J.C., 2003. Quantitative imaging of magnetization transfer using an inversion recovery sequence. Magn. Reson. Med. 49, 501–505.

Goerke, S., Zaiss, M., Bachert, P., 2014. Characterization of creatine guanidinium proton exchange by water-exchange (WEX) spectroscopy for absolute-pH CEST imaging in vitro. NMR Biomed. 27, 507–518.

Goffeney, N., Bulte, J.W., Duyn, J., Bryant, L.H., Jr., van Zijl, P.C., 2001. Sensitive NMR detection of cationic-polymer-based gene delivery systems using saturation transfer via proton exchange. J. Am. Chem. Soc. 123, 8628–8629.

Guivel-Scharen, V., Sinnwell, T., Wolff, S.D., Balaban, R.S., 1998. Detection of proton chemical exchange between metabolites and water in biological tissues. J. Magn. Reson. 133, 36–45.

Haris, M., Cai, K., Singh, A., Hariharan, H., Reddy, R., 2011. In vivo mapping of brain myo-inositol. Neuroimage 54, 2079–2085.

Haris, M., Nanga, R.P., Singh, A., Cai, K., Kogan, F., Hariharan, H., Reddy, R., 2012. Exchange rates of creatine kinase metabolites: feasibility of imaging creatine by chemical exchange saturation transfer MRI. NMR Biomed. 25, 1305–1309.

Haris, M., Nath, K., Cai, K., Singh, A., Crescenzi, R., Kogan, F., Verma, G., Reddy, S., Hariharan, H., Melhem, E.R., Reddy, R., 2013a. Imaging of glutamate neurotransmitter alterations in Alzheimer's disease. NMR Biomed. 26, 386–391.

Haris, M., Singh, A., Cai, K., Kogan, F., McGarvey, J., Debrosse, C., Zsido, G.A., Witschey, W.R., Koomalsingh, K., Pilla, J.J., Chirinos, J.A., Ferrari, V.A., Gorman, J.H., Hariharan, H., Gorman, R.C., Reddy, R., 2014. A technique for in vivo mapping of myocardial creatine kinase metabolism. Nat. Med. 20, 209–214.

Haris, M., Singh, A., Cai, K., Nath, K., Crescenzi, R., Kogan, F., Hariharan, H., Reddy, R., 2013b. MICEST: a potential tool for non-invasive detection of molecular changes in Alzheimer's disease. J. Neurosci. Methods 212, 87–93.

Harrison, R., Bronskill, M.J., Henkelman, R.M., 1995. Magnetization transfer and T2 relaxation components in tissue. Magn. Reson. Med. 33, 490–496.

Henkelman, R.M., 1985. Measurement of signal intensities in the presence of noise in MR images. Med. Phys. 12, 232–233.

Henkelman, R.M., Huang, X., Xiang, Q.S., Stanisz, G.J., Swanson, S.D., Bronskill, M.J., 1993. Quantitative interpretation of magnetization transfer. Magn. Reson. Med. 29, 759–766.

Henkelman, R.M., Stanisz, G.J., Graham, S.J., 2001. Magnetization transfer in MRI: a review. NMR Biomed. 14, 57–64.

Heo, H.Y., Jones, C.K., Hua, J., Yadav, N., Agarwal, S., Zhou, J., van Zijl, P.C., Pillai, J.J., 2016a. Whole-brain amide proton transfer (APT) and nuclear overhauser enhancement (NOE) imaging in glioma patients using low-power steady-state pulsed chemical exchange saturation transfer (CEST) imaging at 7 T. J. Magn. Reson. Imaging 44, 41–50.

Heo, H.Y., Zhang, Y., Burton, T., Jiang, S., van Zijl, P.C.M., Zhou, J., 2017. Improving amide proton transfer (APT) MRI quantification in acute human stroke patients: achieving more pure apt signals and higher detection sensitivity. In: Proceedings of the 24th Annual Meeting of the ISMRM Honolulu, USA. p. 857 (in press).

Heo, H.Y., Zhang, Y., Jiang, S., Lee, D.H., Zhou, J., 2016b. Quantitative assessment of amide proton transfer (APT) and nuclear overhauser enhancement (NOE) imaging with extrapolated semisolid magnetization transfer reference (EMR) signals: II. Comparison of three EMR models and application to human brain glioma at 3 T. Magn. Reson. Med. 75, 1630–1639.

Heo, H.Y., Zhang, Y., Lee, D.H., Hong, X., Zhou, J., 2016c. Quantitative assessment of amide proton transfer (APT) and nuclear overhauser enhancement (NOE) imaging with extrapolated semi-solid magnetization transfer reference (EMR) signals: application to a rat glioma model at 4.7 T. Magn. Reson. Med. 75, 137–149.

Hua, J., Jones, C.K., Blakeley, J., Smith, S.A., van Zijl, P.C., Zhou, J., 2007. Quantitative description of the asymmetry in magnetization transfer effects around the water resonance in the human brain. Magn. Reson. Med. 58, 786–793.

Hwang, T.L., van Zijl, P.C., Mori, S., 1998. Accurate quantitation of water-amide proton exchange rates using the phase-modulated CLEAN chemical EXchange (CLEANEX-PM) approach with a Fast-HSQC (FHSQC) detection scheme. J. Biomol. NMR 11, 221–226.

Jiang, S., Blakeley, J., Eberhart, C., Zhang, Y., Heo, H.-Y., Wen, Z., Blair, L., Qin, H., Lim, M., Quinones-Hinojosa, A., Lee, D.-H., Zhao, X., van Zijl, P.C.M., Zhou, J., 2016a. Image-Guided Stereotactic Biopsy in Patients with Newly Diagnosed Gliomas. In: Proceedings of the 24th Annual Meeting of the ISMRM Singapore.

Jiang, S., Eberhart, C., Blakeley, J., Blair, L., Qin, H., Lim, M., Quinones-Hinojosa, A., Heo, H.-Y., Zhang, Y., Lee, D.-H., Zhao, X., Wen, Z., van Zijl, P.C.M., Zhou, J., 2016b. Amide-Proton-Transfer-Weighted (APTw) MRI as a surrogate biomarker to detect recurrent high-grade gliomas after treatment with chemoradiation: validation by image-guided stereotactic biopsy. In: Proceedings of the 24th Annual Meeting of the ISMRM Singapore, vol. 230.

Jiang, S., Yu, H., Wang, X., Lu, S., Li, Y., Feng, L., Zhang, Y., Heo, H.Y., Lee, D.H., Zhou, J., Wen, Z., 2016c. Molecular MRI differentiation between primary central nervous system lymphomas and high-grade gliomas using endogenous protein-based amide proton transfer MR imaging at 3 T. Eur. Radiol. 26, 64–71.

Jin, T., Wang, P., Zong, X., Kim, S.G., 2013. MR imaging of the amide-proton transfer effect and the pH-insensitive nuclear overhauser effect at 9.4 T. Magn. Reson. Med. 69, 760–770.

Jones, C.K., Huang, A., Xu, J., Edden, R.A., Schar, M., Hua, J., Oskolkov, N., Zaca, D., Zhou, J., McMahon, M.T., Pillai, J.J., van Zijl, P.C., 2013. Nuclear Overhauser enhancement (NOE) imaging in the human brain at 7 T. Neuroimage 77, 114–124.

Jones, C.K., Schlosser, M.J., van Zijl, P.C., Pomper, M.G., Golay, X., Zhou, J., 2006. Amide proton transfer imaging of human brain tumors at 3 T. Magn. Reson Med 56, 585–592.

Kauppinen, R.A., Niskanen, T., Hakumaki, J., Williams, S.R., 1993. Quantitative analysis of 1H NMR detected proteins in the rat cerebral cortex in vivo and in vitro. NMR Biomed. 6, 242–247.

Keupp, J., Eggers, H., 2010. CEST-Dixon MRI for Sensitive and Accurate Measurement of Amide Proton Transfer in Humans at 3 T. In: Proceedings of the 18th Annual Meeting of ISMRM, Stockholm, Sweden, vol. 338.

Kim, M., Gillen, J., Landman, B.A., Zhou, J., van Zijl, P.C., 2009. Water saturation shift referencing (WASSR) for chemical exchange saturation transfer (CEST) experiments. Magn. Reson. Med. 61, 1441–1450.

Kogan, F., Haris, M., Debrosse, C., Singh, A., Nanga, R.P., Cai, K., Hariharan, H., Reddy, R., 2014a. In vivo chemical exchange saturation transfer imaging of creatine (CrCEST) in skeletal muscle at 3 T. J. Magn. Reson. Imaging 40, 596–602.
Kogan, F., Haris, M., Singh, A., Cai, K., Debrosse, C., Nanga, R.P., Hariharan, H., Reddy, R., 2014b. Method for high-resolution imaging of creatine in vivo using chemical exchange saturation transfer. Magn. Reson. Med. 71, 164–172.
Kogan, F., Singh, A., Debrosse, C., Haris, M., Cai, K., Nanga, R.P., Elliott, M., Hariharan, H., Reddy, R., 2013. Imaging of glutamate in the spinal cord using GluCEST. Neuroimage 77, 262–267.
Lauzon, C.B., van Zijl, P., Stivers, J.T., 2011. Using the water signal to detect invisible exchanging protons in the catalytic triad of a serine protease. J. Biomol. NMR 50, 299–314.
Lee, D.H., Heo, H.Y., Zhang, K., Zhang, Y., Jiang, S., Zhao, X., Zhou, J., 2016. Quantitative assessment of the effects of water proton concentration and water T1 changes on amide proton transfer (APT) and nuclear overhauser enhancement (NOE) MRI: the origin of the APT imaging signal in brain tumor. Magn. Reson. Med..
Lee, J.S., Regatte, R.R., Jerschow, A., 2012. Isolating chemical exchange saturation transfer contrast from magnetization transfer asymmetry under two-frequency rf irradiation. J. Magn. Reson. 215, 56–63.
Leigh, R., Knutsson, L., Zhou, J., van Zijl, P.C., 2017. Imaging the physiological evolution of the ischemic penumbra in acute ischemic stroke. J. Cereb. Blood Flow Metab., 271678X17700913.
Liepinsh, E., Otting, G., 1996. Proton exchange rates from amino acid side chains–implications for image contrast. Magn. Reson. Med. 35, 30–42.
Lin, C.Y., Yadav, N.N., Friedman, J.I., Ratnakar, J., Sherry, A.D., van Zijl, P.C., 2012. Using frequency-labeled exchange transfer to separate out conventional magnetization transfer effects from exchange transfer effects when detecting ParaCEST agents. Magn. Reson. Med. 67, 906–911.
Ling, W., Regatte, R.R., Navon, G., Jerschow, A., 2008. Assessment of glycosaminoglycan concentration in vivo by chemical exchange-dependent saturation transfer (gagCEST). Proc. Natl. Acad. Sci. USA 105, 2266–2270.
Ma, B., Blakeley, J.O., Hong, X., Zhang, H., Jiang, S., Blair, L., Zhang, Y., Heo, H.Y., Zhang, M., van Zijl, P.C., Zhou, J., 2016. Applying amide proton transfer-weighted MRI to distinguish pseudoprogression from true progression in malignant gliomas. J. Magn. Reson. Imaging 44, 456–462.
Mori, S., Abeygunawardana, C., van Zijl, P.C., Berg, J.M., 1996a. Water exchange filter with improved sensitivity (WEX II) to study solvent-exchangeable protons. Application to the consensus zinc finger peptide CP-1. J. Magn. Reson. B 110, 96–101.
Mori, S., Berg, J.M., van Zijl, P.C., 1996b. Separation of intramolecular NOE and exchange peaks in water exchange spectroscopy using spin-echo filters. J. Biomol. NMR 7, 77–82.
Morrison, C., Stanisz, G., Henkelman, R.M., 1995. Modeling magnetization transfer for biological-like systems using a semi-solid pool with a super-Lorentzian lineshape and dipolar reservoir. J. Magn. Reson. B 108, 103–113.
Mulkern, R.V., Williams, M.L., 1993. The general solution to the Bloch equation with constant rf and relaxation terms: application to saturation and slice selection. Med. Phys. 20, 5–13.
Narvainen, J., Hubbard, P.L., Kauppinen, R.A., Morris, G.A., 2010. Z-spectroscopy with alternating-phase irradiation. J. Magn. Reson. 207, 242–250.
Nasrallah, F.A., Pages, G., Kuchel, P.W., Golay, X., Chuang, K.H., 2013. Imaging brain deoxyglucose uptake and metabolism by glucoCEST MRI. J. Cereb. Blood Flow Metab. 33, 1270–1278.
Otting, G., Liepinsh, E., Wuthrich, K., 1991. Protein hydration in aqueous solution. Science 254, 974–980.
Park, J.E., Kim, H.S., Park, K.J., Choi, C.G., Kim, S.J., 2015a. Histogram analysis of amide proton transfer imaging to identify contrast-enhancing low-grade brain tumor that mimics high-grade tumor: increased accuracy of MR perfusion. Radiology 277, 151–161.
Park, J.E., Kim, H.S., Park, K.J., Kim, S.J., Kim, J.H., Smith, S.A., 2015b. Pre- and posttreatment glioma: comparison of amide proton transfer imaging with mr spectroscopy for biomarkers of tumor proliferation. Radiology, 142979.
Pekar, J., Jezzard, P., Roberts, D.A., Leigh, J.S., Jr., Frank, J.A., McLaughlin, A.C., 1996. Perfusion imaging with compensation for asymmetric magnetization transfer effects. Magn. Reson Med 35, 70–79.
Pepin, J., Francelle, L., Carrillo-de Sauvage, M.A., de Longprez, L., Gipchtein, P., Cambon, K., Valette, J., Brouillet, E., Flament, J., 2016. In vivo imaging of brain glutamate defects in a knock-in mouse model of Huntington's disease. Neuroimage 139, 53–64.
Pike, G.B., 1996. Pulsed magnetization transfer contrast in gradient echo imaging: a two-pool analytic description of signal response. Magn. Reson. Med. 36, 95–103.
Price, T.B., Gore, J.C., 1998. Effect of muscle glycogen content on exercise-induced changes in muscle T2 times. J Appl. Physiol. 84, 1178–1184, (1985).
Sagiyama, K., Mashimo, T., Togao, O., Vemireddy, V., Hatanpaa, K.J., Maher, E.A., Mickey, B.E., Pan, E., Sherry, A.D., Bachoo, R.M., Takahashi, M., 2014. In vivo chemical exchange saturation transfer imaging allows early detection of a therapeutic response in glioblastoma. Proc. Natl. Acad. Sci. USA 111, 4542–4547.
Sakata, A., Okada, T., Yamamoto, A., Kanagaki, M., Fushimi, Y., Okada, T., Dodo, T., Arakawa, Y., Schmitt, B., Miyamoto, S., Togashi, K., 2015. Grading glial tumors with amide proton transfer MR imaging: different analytical approaches. J. Neurooncol..
Salhotra, A., Lal, B., Laterra, J., Sun, P.Z., van Zijl, P.C., Zhou, J., 2008. Amide proton transfer imaging of 9L gliosarcoma and human glioblastoma xenografts. NMR Biomed. 21, 489–497.
Scheidegger, R., Vinogradov, E., Alsop, D.C., 2011. Amide proton transfer imaging with improved robustness to magnetic field inhomogeneity and magnetization transfer asymmetry using saturation with frequency alternating RF irradiation. Magn. Reson. Med. 66, 1275–1285.
Scheidegger, R., Wong, E.T., Alsop, D.C., 2014. Contributors to contrast between glioma and brain tissue in chemical exchange saturation transfer sensitive imaging at 3 T. Neuroimage 99, 256–268.
Schuenke, P., Windschuh, J., Roeloffs, V., Ladd, M.E., Bachert, P., Zaiss, M., 2016. Simultaneous mapping of water shift and B1 (WASABI)-application to field-inhomogeneity correction of CEST MRI data. Magn. Reson. Med..
Sherry, A.D., Woods, M., 2008. Chemical exchange saturation transfer contrast agents for magnetic resonance imaging. Annu. Rev. Biomed. Eng. 10, 391–411.
Singh, A., Cai, K., Haris, M., Hariharan, H., Reddy, R., 2013. On B1 inhomogeneity correction of in vivo human brain glutamate chemical exchange saturation transfer contrast at 7 T. Magn. Reson. Med. 69, 818–824.
Sled, J.G., Pike, G.B., 2001. Quantitative imaging of magnetization transfer exchange and relaxation properties in vivo using MRI. Magn. Reson. Med. 46, 923–931.
Smith, S.A., Farrell, J.A., Jones, C.K., Reich, D.S., Calabresi, P.A., van Zijl, P.C., 2006. Pulsed magnetization transfer imaging with body coil transmission at 3 T: feasibility and application. Magn. Reson. Med. 56, 866–875.
Snoussi, K., Gillen, J.S., Horska, A., Puts, N.A., Pradhan, S., Edden, R.A., Barker, P.B., 2015. Comparison of brain gray and white matter macromolecule resonances at 3 and 7 T. Magn. Reson. Med. 74, 607–613.
Solomon, I., 1955. Relaxation processes in a system of two spins. Phys. Rev. 99, 559.
Song, X., Gilad, A.A., Joel, S., Liu, G., Bar-Shir, A., Liang, Y., Gorelik, M., Pekar, J.J., van Zijl, P.C., Bulte, J.W., McMahon, M.T., 2012. CEST phase mapping using a length and offset varied saturation (LOVARS) scheme. Magn. Reson. Med. 68, 1074–1086.
Song, X., Xu, J., Xia, S., Yadav, N.N., Lal, B., Laterra, J., Bulte, J.W., van Zijl, P.C., McMahon, M.T., 2015. Multi-echo length and offset varied saturation (MeLOVARS) method for improved CEST imaging. Magn. Reson. Med. 73, 488–496.
Stancanello, J., Terreno, E., Castelli, D.D., Cabella, C., Uggeri, F., Aime, S., 2008. Development and validation of a smoothing-splines-based correction method for improving the analysis of CEST-MR images. Contrast Media Mol. Imaging 3, 136–149.
Stanisz, G.J., Kecojevic, A., Bronskill, M.J., Henkelman, R.M., 1999. Characterizing white matter with magnetization transfer and T(2). Magn. Reson. Med. 42, 1128–1136.
Stanisz, G.J., Odrobina, E.E., Pun, J., Escaravage, M., Graham, S.J., Bronskill, M.J., Henkelman, R.M., 2005. T1, T2 relaxation and magnetization transfer in tissue at 3 T. Magn. Reson. Med. 54, 507–512.
Sun, P.Z., Zhou, J., Sun, W., Huang, J., van Zijl, P.C., 2007. Detection of the ischemic penumbra using pH-weighted MRI. J Cereb. Blood Flow Metab. 27, 1129–1136.
Swanson, S., Pang, Y., 2003. MT is symmetric but shifted with respect to water. In: Proceedings of the 11th Annual Meeting ISMRM.
Swanson, S.D., 1998. Protein mediated magnetic coupling between lactate and water protons. J. Magn. Reson. 135, 248–255.
Swanson, S.D., Malyarenko, D.I., Fabiilli, M.L., Welsh, R.C., Nielsen, J.F., Srinivasan, A., 2016. Molecular, dynamic, and structural origin of inhomogeneous magnetization transfer in lipid membranes. Magn. Reson. Med..
Togao, O., Yoshiura, T., Keupp, J., Hiwatashi, A., Yamashita, K., Kikuchi, K., Suzuki, Y., Suzuki, S.O., Iwaki, T., Hata, N., Mizoguchi, M., Yoshimoto, K., Sagiyama, K., Takahashi, M., Honda, H., 2014. Amide proton transfer imaging of adult diffuse gliomas: correlation with histopathological grades. Neuro Oncol. 16, 441–448.
van Zijl, P.C., Jones, C.K., Ren, J., Malloy, C.R., Sherry, A.D., 2007. MRI detection of glycogen in vivo by using chemical exchange saturation transfer imaging (glycoCEST). Proc. Natl. Acad. Sci. USA 104, 4359–4364.
van Zijl, P.C., Sehgal, A.A., 2016. Proton chemical exchange saturation transfer (CEST) MRS and MRI. eMagRes 5, 1–26. http://dx.doi.org/10.1002/9780470034590.emrstm9780470031482.
van Zijl, P.C., Yadav, N.N., 2011. Chemical exchange saturation transfer (CEST): what is in a name and what isn't? Magn. Reson. Med. 65, 927–948.
van Zijl, P.C., Zhou, J., Mori, N., Payen, J.F., Wilson, D., Mori, S., 2003. Mechanism of magnetization transfer during on-resonance water saturation. A new approach to detect mobile proteins, peptides, and lipids. Magn. Reson. Med. 49, 440–449.
Vinogradov, E., Soesbe, T.C., Balschi, J.A., Sherry, A.D., Lenkinski, R.E., 2012. pCEST: positive contrast using chemical exchange saturation transfer. J. Magn. Reson. 215, 64–73.
Walker-Samuel, S., Ramasawmy, R., Torrealdea, F., Rega, M., Rajkumar, V., Johnson, S.P., Richardson, S., Goncalves, M., Parkes, H.G., Arstad, E., Thomas, D.L., Pedley, R.B., Lythgoe, M.F., Golay, X., 2013. In vivo imaging of glucose uptake and metabolism in tumors. Nat. Med. 19, 1067–1072.
Ward, K.M., Aletras, A.H., Balaban, R.S., 2000. A new class of contrast agents for MRI based on proton chemical exchange dependent saturation transfer (CEST). J. Magn. Reson. 143, 79–87.
Wei, W., Jia, G., Sammet, S., Wassenaar, P., Zhou, J., Knopp, M.V., 2010. Improving amide proton transfer imaging with dual echo B0 mapping for field inhomogeneity correction at 3 T. In: Proceedings of the 18th Annual Meeting of ISMRM, Stockholm, Sweden, vol. 2986.
Wen, Z., Hu, S., Huang, F., Wang, X., Guo, L., Quan, X., Wang, S., Zhou, J., 2010. MR imaging of high-grade brain tumors using endogenous protein and peptide-based contrast. Neuroimage 51, 616–622.
Windschuh, J., Zaiss, M., Meissner, J.E., Paech, D., Radbruch, A., Ladd, M.E., Bachert, P., 2015. Correction of B1-inhomogeneities for relaxation-compensated CEST imaging at 7 T. NMR Biomed. 28, 529–537.
Woessner, D.E., Zhang, S., Merritt, M.E., Sherry, A.D., 2005. Numerical solution of the Bloch equations provides insights into the optimum design of PARACEST agents for MRI. Magn. Reson. Med. 53, 790–799.
Wolff, S.D., Balaban, R.S., 1989. Magnetization transfer contrast (MTC) and tissue water proton relaxation in vivo. Magn. Reson. Med. 10, 135–144.

Xu, J., Chan, K.W., Xu, X., Yadav, N., Liu, G., van Zijl, P.C., 2017. On-resonance variable delay multipulse scheme for imaging of fast-exchanging protons and semisolid macromolecules. Magn. Reson. Med. 77, 730–739.
Xu, J., Yadav, N.N., Bar-Shir, A., Jones, C.K., Chan, K.W., Zhang, J., Walczak, P., McMahon, M.T., van Zijl, P.C., 2014. Variable delay multi-pulse train for fast chemical exchange saturation transfer and relayed-nuclear overhauser enhancement MRI. Magn. Reson. Med. 71, 1798–1812.
Xu, X., Chan, K.W., Knutsson, L., Artemov, D., Xu, J., Liu, G., Kato, Y., Lal, B., Laterra, J., McMahon, M.T., van Zijl, P.C., 2015a. Dynamic glucose enhanced (DGE) MRI for combined imaging of blood-brain barrier break down and increased blood volume in brain cancer. Magn. Reson. Med..
Xu, X., Yadav, N., Knutsson, L., Hua, J., Kalyani, R., Hall, E., Laterra, J., Blakeley, J., Strowd, R., Pomper, M., Barker, P., Chan, K.W., Liu, G., McMahon, M.T., Stevens, R.D., van Zijl, P.C., 2015b. Dynamic glucose-enhanced (DGE) MRI: translation to human scanning and first results in glioma patients. Tomography 1, 105–114.
Xu, X., Yadav, N.N., Zeng, H., Jones, C.K., Zhou, J., van Zijl, P.C., Xu, J., 2016. Magnetization transfer contrast-suppressed imaging of amide proton transfer and relayed nuclear overhauser enhancement chemical exchange saturation transfer effects in the human brain at 7 T. Magn. Reson. Med. 75, 88–96.
Yadav, N.N., Jones, C.K., Xu, J., Bar-Shir, A., Gilad, A.A., McMahon, M.T., van Zijl, P.C., 2012. Detection of rapidly exchanging compounds using on-resonance frequency-labeled exchange (FLEX) transfer. Magn. Reson. Med. 68, 1048–1055.
Yang, X., Song, X., Li, Y., Liu, G., Ray Banerjee, S., Pomper, M.G., McMahon, M.T., 2013. Salicylic acid and analogues as diaCEST MRI contrast agents with highly shifted exchangeable proton frequencies. Angew. Chem. Int. Ed. Engl. 52, 8116–8119.
Zaiss, M., Bachert, P., 2013a. Chemical exchange saturation transfer (CEST) and MR Z-spectroscopy in vivo: a review of theoretical approaches and methods. Phys. Med. Biol., 58, (R221-269).
Zaiss, M., Bachert, P., 2013b. Exchange-dependent relaxation in the rotating frame for slow and intermediate exchange – modeling off-resonant spin-lock and chemical exchange saturation transfer. NMR Biomed. 26, 507–518.
Zaiss, M., Windschuh, J., Paech, D., Meissner, J.E., Burth, S., Schmitt, B., Kickingereder, P., Wiestler, B., Wick, W., Bendszus, M., Schlemmer, H.P., Ladd, M.E., Bachert, P., Radbruch, A., 2015a. Relaxation-compensated CEST-MRI of the human brain at 7 T: unbiased insight into NOE and amide signal changes in human glioblastoma. Neuroimage 112, 180–188.
Zaiss, M., Xu, J., Goerke, S., Khan, I.S., Singer, R.J., Gore, J.C., Gochberg, D.F., Bachert, P., 2014. Inverse Z-spectrum analysis for spillover-, MT-, and T1 -corrected steady-state pulsed CEST-MRI–application to pH-weighted MRI of acute stroke. NMR Biomed. 27, 240–252.
Zaiss, M., Zu, Z., Xu, J., Schuenke, P., Gochberg, D.F., Gore, J.C., Ladd, M.E., Bachert, P., 2015b. A combined analytical solution for chemical exchange saturation transfer and semi-solid magnetization transfer. NMR Biomed. 28, 217–230.
Zhang, X.Y., Wang, F., Afzal, A., Xu, J., Gore, J.C., Gochberg, D.F., Zu, Z., 2016a. A new NOE-mediated MT signal at around -1.6ppm for detecting ischemic stroke in rat brain. Magn. Reson Imaging 34, 1100–1106.
Zhang, X.Y., Wang, F., Jin, T., Xu, J., Xie, J., Gochberg, D.F., Gore, J.C., Zu, Z., 2016b. MR imaging of a novel NOE-mediated magnetization transfer with water in rat brain at 9.4 T. Magn. Reson. Med..
Zhang, X.Y., Wang, F., Li, H., Xu, J., Gochberg, D.F., Gore, J.C., Zu, Z., 2017a. Accuracy in the quantification of chemical exchange saturation transfer (CEST) and relayed nuclear Overhauser enhancement (rNOE) saturation transfer effects. NMR Biomed..
Zhang, X.Y., Wang, F., Li, H., Xu, J., Gochberg, D.F., Gore, J.C., Zu, Z., 2017b. CEST imaging of fast exchanging amine pools with corrections for competing effects at 9.4 T. NMR Biomed..
Zhao, X., Wen, Z., Zhang, G., Huang, F., Lu, S., Wang, X., Hu, S., Chen, M., Zhou, J., 2013. Three-dimensional turbo-spin-echo amide proton transfer MR imaging at 3-T and its application to high-grade human brain tumors. Mol. Imaging Biol. 15, 114–122.
Zhou, J., Blakeley, J.O., Hua, J., Kim, M., Laterra, J., Pomper, M.G., van Zijl, P.C., 2008. Practical data acquisition method for human brain tumor amide proton transfer (APT) imaging. Magn. Reson. Med. 60, 842–849.
Zhou, J., Lal, B., Wilson, D.A., Laterra, J., van Zijl, P.C., 2003a. Amide proton transfer (APT) contrast for imaging of brain tumors. Magn. Reson. Med. 50, 1120–1126.
Zhou, J., Payen, J.F., Wilson, D.A., Traystman, R.J., van Zijl, P.C., 2003b. Using the amide proton signals of intracellular proteins and peptides to detect pH effects in MRI. Nat. Med. 9, 1085–1090.
Zhou, J., Tryggestad, E., Wen, Z., Lal, B., Zhou, T., Grossman, R., Wang, S., Yan, K., Fu, D.X., Ford, E., Tyler, B., Blakeley, J., Laterra, J., van Zijl, P.C., 2011. Differentiation between glioma and radiation necrosis using molecular magnetic resonance imaging of endogenous proteins and peptides. Nat. Med 17, 130–134.
Zhou, J., van Zijl, P., 2006. Chemical exchange saturation transfer imaging and spectroscopy. Prog. NMR Spectr. 48, 109–136.
Zhou, J., van Zijl, P.C., 2011. Defining an acidosis-based ischemic penumbra from pH-weighted MRI. Transl. Stroke Res. 3, 76–83.
Zhou, J., Wilson, D.A., Sun, P.Z., Klaus, J.A., Van Zijl, P.C., 2004. Quantitative description of proton exchange processes between water and endogenous and exogenous agents for WEX, CEST, and APT experiments. Magn. Reson. Med. 51, 945–952.
Zhou, J., Zhu, H., Lim, M., Blair, L., Quinones-Hinojosa, A., Messina, S.A., Eberhart, C.G., Pomper, M.G., Laterra, J., Barker, P.B., van Zijl, P.C., Blakeley, J.O., 2013. Three-dimensional amide proton transfer MR imaging of gliomas: initial experience and comparison with gadolinium enhancement. J. Magn. Reson. Imaging 38, 1119–1128.
Zu, Z., Janve, V.A., Li, K., Does, M.D., Gore, J.C., Gochberg, D.F., 2012. Multi-angle ratiometric approach to measure chemical exchange in amide proton transfer imaging. Magn. Reson. Med. 68, 711–719.
Zu, Z., Janve, V.A., Xu, J., Does, M.D., Gore, J.C., Gochberg, D.F., 2013. A new method for detecting exchanging amide protons using chemical exchange rotation transfer. Magn. Reson. Med. 69, 637–647.